TECHNICAL UNIVERSITY OF LODZ
FACULTY OF MECHANICAL ENGINEERING
Division of Dynamics

Błażej Witkowski

DOCTORAL THESIS

SYNCHRONIZATION OF COUPLED SPHERICAL PENDULA

SUPERVISOR:
Prof. dr hab. inż. Tomasz Kapitaniak

AXUILIARY SUPERVISOR:
Dr inż. Łukasz Borkowski

INNOVATIVE ECONOMY
NATIONAL COHESION STRATE
FNP
Foundation for Polish Science
EUROPEAN UNION
UROPEAN REGIONAL
EVELOPMENT FUND

ŁÓDŹ 2014

Abstract

The doctoral dissertation contains such issues as: synchronization of dynamic systems, non-linear dynamics and modelling. The aim of this study is to obtain the types of synchronization of the system composed of two spherical rotating pendula coupled by a rigid beam. The beam is attached to the ends of two massless and inextensible strings. At both ends of the beam two identical pendula are suspended.

Different mathematical models of the system have been introduced: (i) the beam defined in the Cartesian coordinates using the Lagrange multipliers; (ii) the beam defined in the spherical and Cartesian coordinates using the Lagrange multipliers; (iii) the beam defined in the spherical coordinates. Based on the Lagrange equation of the second type the coupled ordinary differential equations of the second order have been derived. The behavior of the mathematical models has been compared with the behavior of the experimental one. The best mathematical model i.e., one with the beam described in the spherical coordinates, has been chosen for further investigation.

First, system has been simplified to a zero-length beam to determine the non-linear normal modes. Then small amplitudes of the motion of the pendula have been assumed. These assumptions allow the analytical derivation of three normal modes: (i) the phase shift between the pendula is π, they rotate in the same direction, the beam is at rest; (ii) the beam and the pendula rotate in-phase in the same direction; (iii) the beam and the pendula rotate in the same direction but the phase shift between the pendula and the beam is π. Using the Newton-Raphson algorithm the obtained solutions have been corrected for larger amplitudes. In the first mode a pitchfork bifurcation has been observed, which causes the appearance of nonsymmetrical periodic solution and destabilization of initial symmetrical one.

The viscous damping has been modelled, in such a way that both pendula have been equally damped. The constant force has been applied to each pendulum, which is perpendicular to its projection on the XY plane. The numerical analysis of the initial conditions and excitations of the system have been performed. The following observations have been made: (i) when the initial conditions of the pendula are different but their velocities cause the rotation in the same direction, the pendula obtain the second normal mode and the synchronization between them is complete; (ii) if the velocity causes rotation in the opposite direction, first normal mode appears, and the pendula spin in different

directions with the phase shift between them equal to π. In the case (ii) the ends of the beam follow their respective pendula causing the rotation of the beam around the mass center. The practical synchronization between the pendula is observed. Finally, the system with harmonic excitation has been considered. The resonance diagram shows that: (i) if the amplitude of excitation increases, the resonant frequency increases; (ii) if the beam's strings increase, the resonant frequency decreases.

The real system consisting of two coupled spherical pendula has been built. As the excited spherical pendula we use the aircraft toys with electric motors. The results of the numerical analysis have been confirmed.

Acknowledgments

This research has been performed at Lodz University of Technology at Division of Dynamics. This work has been supported by the Foundation for Polish Science, Team Program under project TEAM/2010/5/5.

I would like to thank my supervisor, Professor Tomasz Kapitaniak, for support and good advises given me during my study. Thanks are also extended to Professor Jarosław Strzałko, who has provided many helpful tips to obtain mathematical model of the system. I would like to thank Dr. Awadhesh Prasad for discussions and for fruitful collaboration. I am also grateful to Professor Krzysztof Czołczyński. Even somebody who lives on another planet can bring you down to Earth. Special thanks are given to Professor Przemysław Perlikowski, who has been helping me a lot in numerical research all the time. Thanks are also due to Dr. Jerzy Wojewoda for his help in making films and photographs of the real system. I would like to thank my colleagues Piotr Brzeski, Anna Karmazyn, Piotr Kołuda, Krzysztof Jankowski, Michał Marszal, sometimes even simple thought can help to move forward.

I really don't know how to thank my wife Joanna. She always has been there for me and she has encouraged me. My parents, relatives and friends – thank you for everything. At last I would like to thank my cat Frida, she was warming my legs up in the cool evenings, when I was doing this research.

Błażej Witkowski
Lodz, Poland, May 2014

Appended papers

Paper A

B. Witkowski, *"Modelling of the dynamics of two coupled spherical pendula"*, The European Physical Journal Special Topics (2014)

Abstract:

We study the dynamics of the system of two spherical pendula mounted to the rigid beam which hang from the unmovable frame. Using Langrange's multipliers the equations of motion have been derived. We identify two synchronous states in which pendula rotate in the same or different directions. The results of numerical simulations have been confirmed in the simple experiment.

Paper B

B. Witkowski, P. Perlikowski, A. Prasad,T. Kapitaniak,*"The dynamics of co- and counter rotating coupled spherical pendulums"*, The European Physical Journal Special Topics (2014)

Abstract:

The dynamics of co- and counter-rotating coupled spherical pendula (two lower pendula are mounted at the end of the upper pendulum) is considered. Linear mode analysis shows the existence of three rotating modes. The linear modes allow us to understand the nonlinear normal modes, which are visualized in frequency-energy plots. With the increase of energy in one mode we observe a symmetry breaking pitchfork bifurcation. In the second part of the paper we consider energy transfer between pendula having different energies. The results for co-rotating (all pendula rotate in the same direction) and counter-rotating motion (one of lower pendula rotates in the opposite direction) are presented. In general, the energy fluctuations in counter-rotating pendula are found to be higher than in the co-rotating case.

Contents

Nomenclature

0.1 Notation

$x_i,\ y_i,\ z_i$ – Cartesian coordinates of i-th point of the system

$\alpha,\ \beta,\ \gamma$ – independent variables describing beam's motion

$\alpha_i,\ \beta_i$,– independent variables describing i-th pendulum's motion

$\mathcal{F}_i$ – i-th pendulum's excitation

$F_i,\ \omega$ – amplitude and frequency of i-th pendulum's excitation

c_f – dumping coefficient

M – beam's mass

b – beam's length

l – beam's stings length

m – i-th pendulum's mass

h – i-th pendulum's length

0.2 Abbreviations

DOF – degree of freedom

ICs – initial conditions

CS – complete synchronization

ICS – imperfect complete synchronization

PS – phase synchronization

APS – anti-phase synchronization

CO – co-rotating, rotating in the same direction

CU – counter-rotating, rotating in the opposite direction

Chapter 1

Introduction

In XVII-th century Christian Huygens, as a first scientist, showed that coupled clocks (hanging from a common support) were synchronized [1, 2]. Nowadays many researchers repeat Huygens experiment and try to explain the mechanism of synchronization [1, 2, 3].

Currently, there is a great number of research on the coupled pendula [1-12]. However, most of them are devoted to the planar motion of oscillating [1-12] or rotating pendula [5, 7].

The dynamics of double pendulum has been considered in Ref. [13] where the author used the model consisting of two rigid rods with elastic joints with the force acting parallely to lower pendulum. The detailed stability analysis based on the center manifold theorem has been considered for hanging down position. Here, the period motion under the varying external force and damping coefficient have been studied.

Lee et al. [14] analyzed the global nonlinear stable manifolds of the spherical pendulum hyperbolic equilibrium with closed loop attitude control. Olssen [15, 16] has considered the dynamics of the spherical pendulum. For the small pendulum's motion the derived equation of motion has been solved analytically using Lindstedt-Poincare method.

The phenomena of spherical pendula synchronization has been noticed by Priest and Poth [17]. During "My Fair Lady" drama two actors were swinging on a swing. The ends of the swigs were suspended to the ends of the movable beam. Priest and Poth observed the same phenomena in the laboratory experiment with two spherical pendula and they made an attempt to model such a system. They focused only on the small oscillations along x-axis. The considered system is highly nonlinear and the full system can induce many interesting phenomena.

1.1 Object of the Study

The considered system is composed of a beam and two spherical pendula as presented in Figure1.1.1 . The beam of mass M is attached to the ends of a

massless and inextensible strings, each of them has length l. At the ends of the beam two identical pendula are suspended, each of length h and mass m.

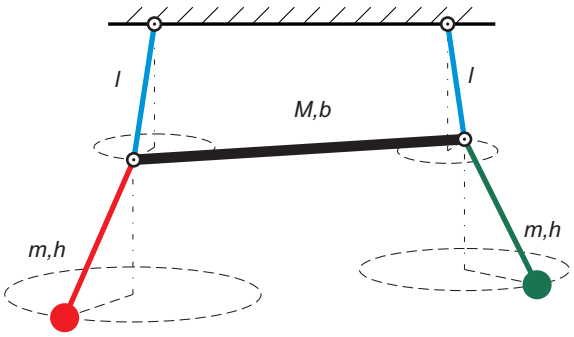

Figure 1.1.1: Model of the spherical pendula coupled by the beam.

Both pendula are externally excited.
In our studies the rotational motion of the pendula is considered.

1.2 The Doctoral Thesis and Main Objective

The thesis was formulated as follows:

"Coupled spherical pendula can synchronize. Different types of synchronization can be identified. The change of the initial conditions and the type of an excitation in the system of the coupled spherical pendula results in qualitative changes in the pendula's dynamics and the type of the synchronization between them."

In the presented doctoral dissertation the dynamics of two coupled spherical pendula have been studied. The general objectives are:

- derive mathematical model of the system;
- calculate periodic rotational solutions;
- identify types of synchronization;
- investigate the influence of initial conditions on the type of synchronization;
- investigate the influence of different excitations on the type of synchronization.
- built a physical model of the system and observe its behavior;

1.3 Thesis Organization

The Thesis is organized as follows. The methodology of research is introduced in Chapter 2. The numerical and experimental analysis have been presented. Section 3.1 contains the derivation of the considered model of the coupled spherical pendula. In Section 3.2 the shape of linear normal mode of the simplified system is obtained. In next section the dumping of the system is considered. In Section 3.3 various excitations are studied. The conclusions of the results are summarized in Chapter 4. In the last chapter future recommendations for future work are presented. At the end of this dissertation the published papers on the considered problems are included.

Chapter 2

Methodology

2.1 Experimental Observation

We have built the real system shown in Fig.2.1.2. We consider the pendula of the lengths $h = 0.5$ [m] and masses $m = 0.096$ [kg] which hang from the beam of the length $b = 1.0$ [m] and mass $M = 0.5$ [kg]. The beam hangs from the unmovable base on the massless strings of length $l = 0.35$ [m] connected to its ends. We have used toy airplanes as constant force that externally excited pendula.

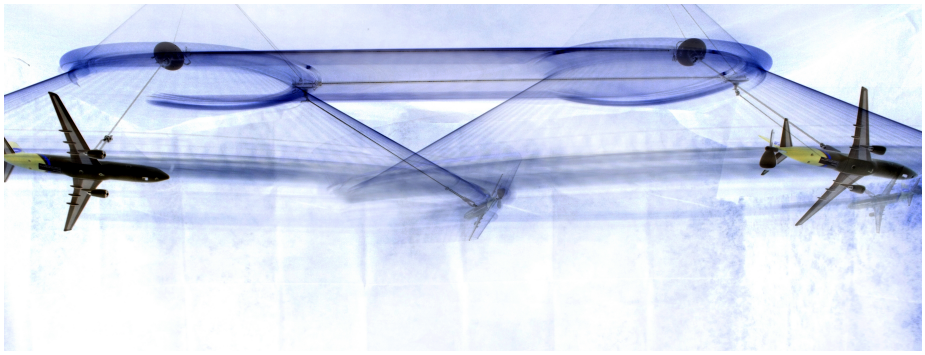

Figure 2.1.1: The real system – general view.

The system behavior has been video recorded and the beam and pendula's trajectories have been determined using image analysis software *Kinovea*. The real system has been used to obtain the qualitative results of the types of motion. To measure the trajectories of the pendula we need complex measuring devices.

The detailed quantified analysis of the system's dynamics will be performed in future works.

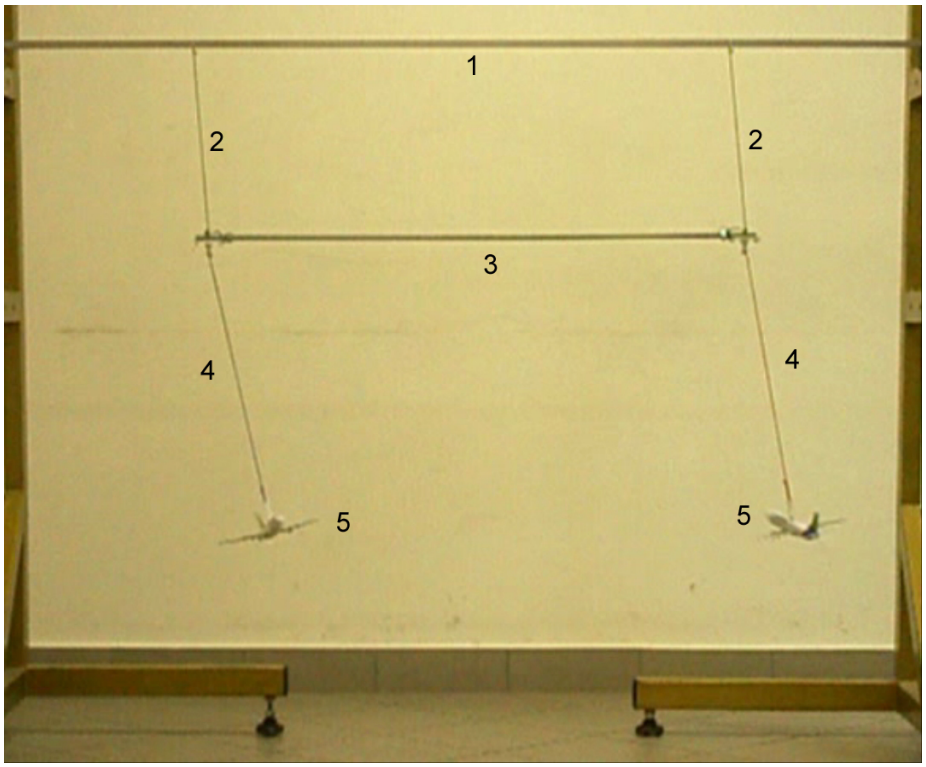

Figure 2.1.2: The real system composed of coupled pendula: (1) support, (2) strings of length $l = 0.35$ [m], (3) a beam of mass $M = 0.5289$ [kg] and length $b = 1$ [m], (4) strings of length $h = 0.5$ [m], (5) toy airplanes as spherical pendula, each of mass $m = 0.096$ [kg] and force $F = 0.0206$ [N].

Two types of stable synchronous motion have been identified as shown in **paper A**. In the first type both pendula synchronize in-phase and rotate in the same direction and we observe in-phase synchronization of the beam and the pendula motion. In the second type the pendula synchronize in anti-phase and rotate in the opposite directions. The performed experiments have not revealed any other stable types of pendula rotating motion.

The same values of parameters (e.g. mass, length, force) have been used in numerical calculations.

Figure 2.1.3: Synchronous motion in the same direction.

Figure 2.1.4: (continue Fig 2.1.3) Synchronous motion in the same direction.

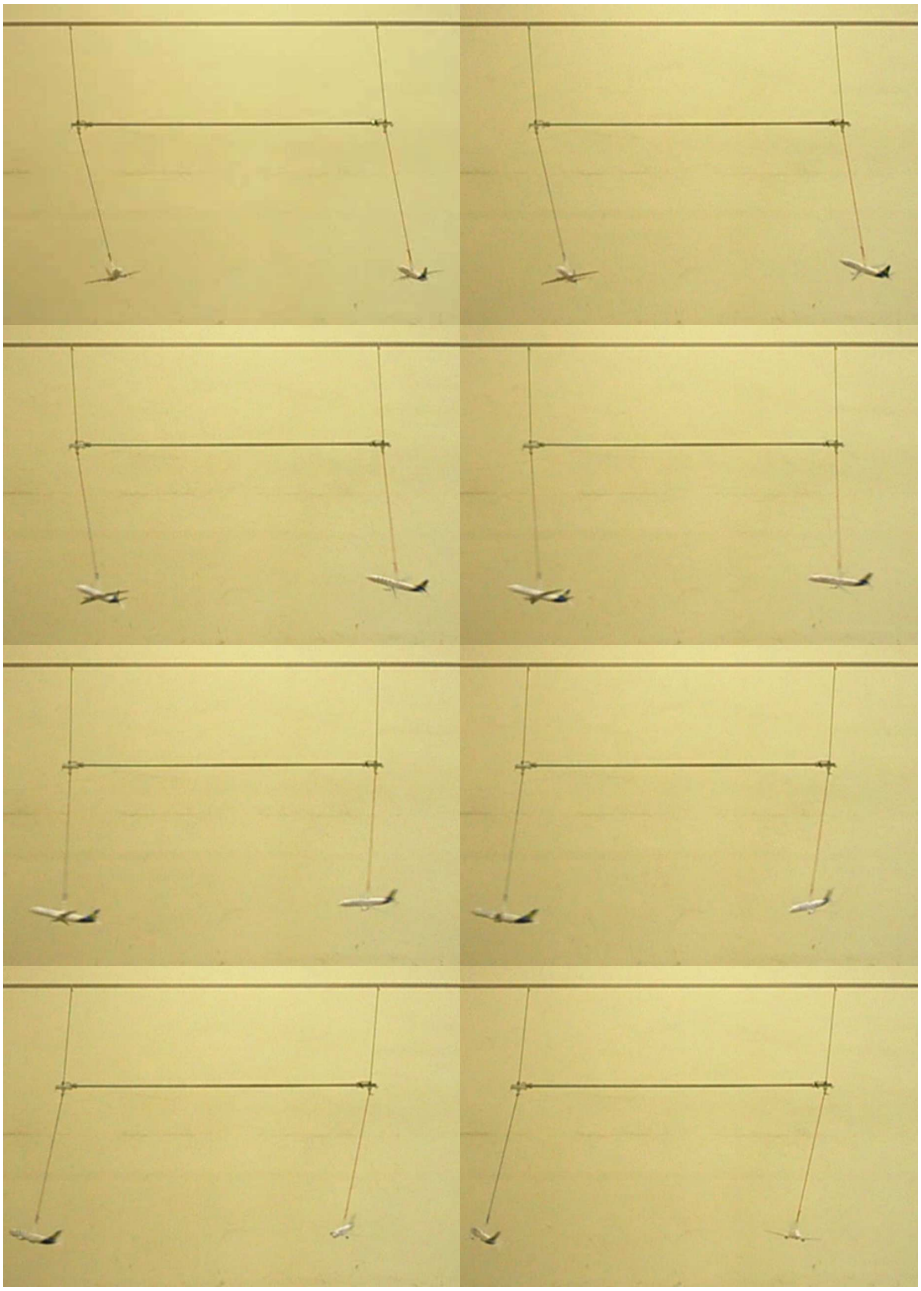

Figure 2.1.5: Synchronous motion in the opposite direction.

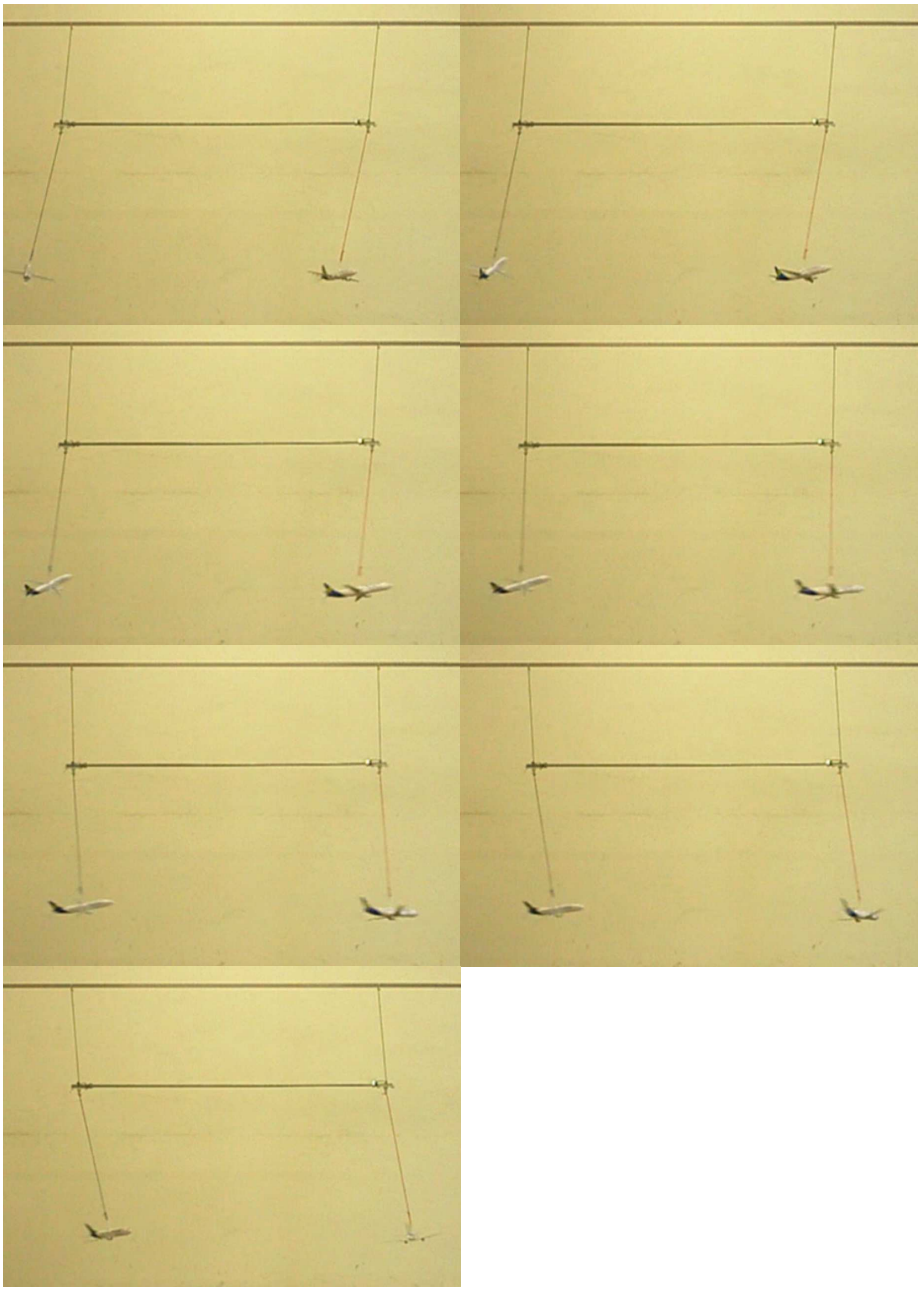

Figure 2.1.6: (continue Fig 2.1.5) Synchronous motion in the opposite direction.

2.2 Numerical Analysis

The ODEs describing the motion of the coupled spherical pendula have been integrated by Runge-Kutta-Fehlberg method [4,5]. All numerical calculations have been done by the author's computer programs which were written in C language.

Due to complexity of the system the propriety of numerical integration has to be checked. In Hamiltonian system the total energy has been measured. Its value was constant with 10^{-6} precision.

The initial conditions for linear modes have been used in full system to obtain nonlinear normal modes. It has caused quasiperiodic orbit (KAM tori) . To correct the obtained solution into periodic one Newton-Raphson algorithm has been applied. The description of its method can be found in [18]. As a correction error the following function has been used:

$$err = \sum_{i=1}^{n} \left(\varphi_i(t+T) - \varphi_i(t)\right)^2 \quad ,$$

where φ_i – i-th value of the state vector of the system (including velocity), T– the period of the system.

The damping coefficient has been calculated as 0.01 of critical damping $c_f = 0.01\sqrt{gl}$. The next logarithmic decrement of the damping of the numerical system has been compared to the logarithmic decrement of damping of the experimental one. The results have been the same.

During numerical examination of the system such diagrams have been done: the bifurcation diagram, the basin of attraction, the resonance diagram. The bifurcation diagram is a set of Poincare sections for bifurcation parameter. For excitation as a force with constant value Poincare sections have been done in the following way: due to constant value of the force there is no frequency of excitation so referential pendulum has been chosen, when one of the chosen variable changes the value from plus to minus then the value of the state vector has been determined. With regard to numerical integration, point of intersection depends on integration step. So changeable step has been used, to obtain intersection point with 10^{-8} precision. The initial conditions in each step on the bifurcation diagram have been taken as a last value of state vector in the previous step. Therefore, one can obtain how the attractor is changing.

Chapter 3

Analysis

In this chapter the mathematical model is derived. First ODEs describing the system's motion are introduced. The full description of the derivation of equations of motion is shown in **paper A**. In Section 3.1 only the Cartesian coordinates will be presented. Next shape of linear and nonlinear normal modes will be obtained in Section 3.2. The details of linear and nonlinear normal modes are presented in **paper B**. Therefore, one can know the possible configurations of the system of the periodic solution. To make the mathematical model as similar as possible to the real one damping and excitation must be added. The numerical analysis deals only with the periodic solutions. For constant force basins of CU and CO solutions will be presented in Section 3.4.1. The change of the length of the beam's string will also give very interesting results. In Section 3.4.2 harmonic excitation will be analyzed. The behavior of the resonant frequency will be shown in the resonant diagram.

3.1 Mathematical Model

To derived the equations of motion we have to make a few assumptions and simplifications. The solid beam is considered as the system of 3 points with mass distributed in the following manner: 1/6 at the ends and 2/3 in the middle. The full system has 7 degrees of freedom, so 7 independent variables are needed. If we describe the position of the pendula by spherical coordinates, we get 4 independent variables, 2 for each pendulum. The question arises how to describe the beam's motion.

We need to describe the positions of 3 beam's points (end and middle). The position of the middle point is average of the positions of the beam's ends. Point A as in Fig 3.1.1 can be described in the same manner as pendula. To obtain the position of end B let us divide the beam hanged on the strings into two triangle: $AO1O2$ and $ABO2$. The angle between them is the third independent variable.

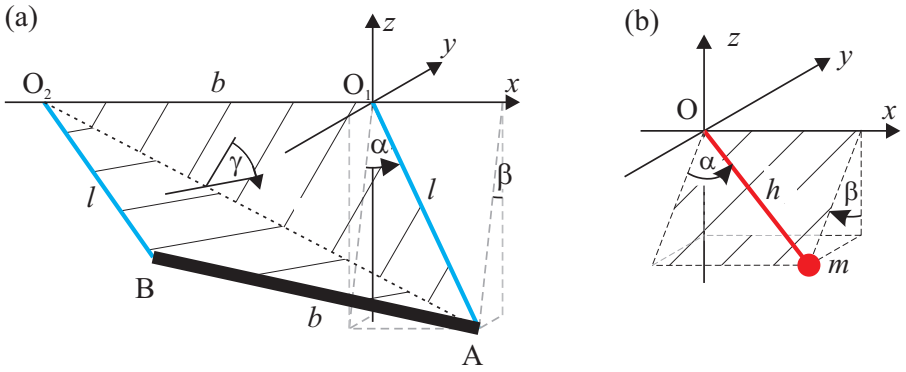

Figure 3.1.1: (a) model of the beam; (b) spherical pendulum described in the changed spherical coordinates.

Than Cartesian coordinates of each point of the system is given by the following form:

$$x_A = l\sin[\alpha], \quad y_A = l\cos[\alpha]\sin[\beta], \quad z_A = -l\cos[\alpha]\cos[\beta],$$

$$x_B = \frac{l(b + l\sin[\alpha])(l + b\sin[\alpha])}{d^2} - \frac{l^2 b\cos[\alpha]^2\cos[\gamma]}{d^2} - b,$$
$$y_B = \frac{l\cos[\alpha]((b\cos[\gamma](b + l\sin[\alpha]) + l(l + b\sin[\alpha]))\sin[\beta] + d\,b\cos[\beta]\sin[\gamma])}{d^2},$$
$$z_B = -\frac{l\cos[\alpha](\cos[\beta](b\cos[\gamma](b + l\sin[\alpha]) + l(l + b\sin[\alpha])) - d\,b\sin[\beta]\sin[\gamma])}{d^2}.$$

$$x_D = h\sin[\alpha_1] + x_A, \quad y_D = h\cos[\alpha_1]\sin[\beta_1] + y_A, \quad z_D = -h\cos[\alpha_1]\cos[\beta_1] + z_A,$$
$$x_E = h\sin[\alpha_2] + x_B, \quad y_E = h\cos[\alpha_2]\sin[\beta_2] + y_B, \quad z_E = -h\cos[\alpha_2]\cos[\beta_2] + z_B.$$

Full derivation of these coordinates are shown in **paper A.** Next, the velocity of each point can be calculated to obtain kinetic energy of the whole system. Using the formula of kinetic and potential energy one may obtain the second order ODEs describing the motion of the system from Lagrange equations of the second kind.

3.2 Linear and nonlinear normal modes

Due to system's complexity it is hard to determine normal modes for full system. Therefore, zero-length beam has been assumed as a simplification of the system. This assumption causes no information about the third variable of the beam. Next small motion has been considered. Three normal modes as in Fig. 3.2.1 have been obtained analytically:

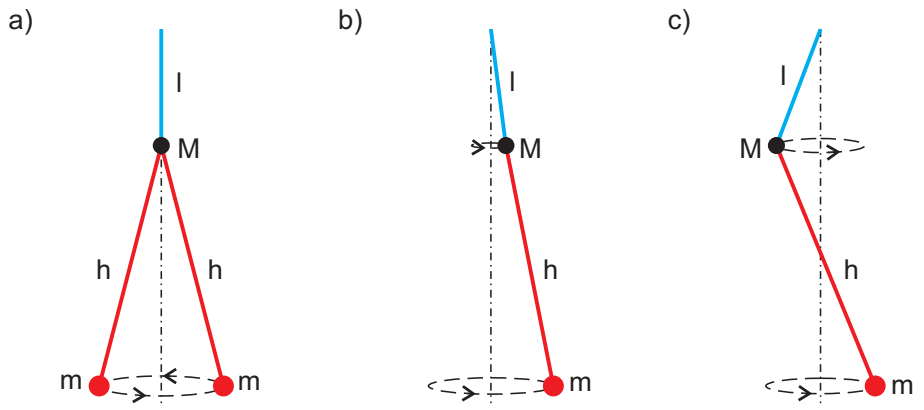

Figure 3.2.1: Shapes of normal modes.

1. the phase shift between the pendula is equal to π, they rotate in the same direction, the beam is at rest;
2. the beam and the pendula rotate in-phase in the same direction;
3. the beam and the pendula rotate in the same direction but the phase shift between the pendula and the beam is equal to π.

For all three modes the dynamics on a KAM tori is observed . Based on the above normal modes and using the correction algorithm of Newton-Raphson, one can obtain the non-linear normal modes for larger energies. All calculations of linear normal modes are shown in **paper B**.

3.3 Damping

So far we have considered the Hamiltonian system. Now we introduce the viscous damping to the system. As third variable γ is virtual, the damping function has to equally damp nodes: *A*,*B* and *O1*, *O2* (see Fig. 3.1.1). The dissipation function has been constructed as follows:

$$\begin{aligned} R(q,\dot{q}) \quad &= \tfrac{1}{2} C_f \left(\dot{\alpha}^2 + \dot{\beta}^2 + \dot{\alpha}^{*2} + \dot{\beta}^{*2} \left(\cos\left(\beta - \beta_1\right) \dot{\alpha} - \dot{\alpha_1} \right)^2 + \right. \\ &\left. + \left(\dot{\beta} - \dot{\beta_1} \right)^2 + \left(\cos\left(\beta^* - \beta_2\right) \dot{\alpha}^* - \dot{\alpha_2} \right)^2 + \left(\dot{\beta}^* - \dot{\beta_1} \right)^2 \right), \end{aligned}$$

where $\dot{\alpha}^*$ and $\dot{\beta}^*$are the velocities of the additional variables, which describe position of point B in the same way as variables α and β describe position of point A. Details can be found in **paper A**.

3.4 External Excitation

In our studies various types of external excitation such as constant force, harmonic and van der Pol's type have been considered.

3.4.1 Force with constant value

Contrary to harmonic excitation, constant force in three dimensional system can cause such phenomena as: complete or practical synchronization, phase or anti-phase synchronization or even chaotic motion. In the real system toy airplanes with DC motors have been used as excitation. During the motion the force is acting on to pendulum in various directions. But after some transient time the pendulum's rotation is stable and there are no fluctuations. That is why the simplified model of this type of excitation is studied. Let us consider the constant force perpendicular to its projection on the XY plane by the following formula:

$$\begin{aligned}\mathcal{F}_1 &= \frac{F_1}{\sqrt{(x_D-x_A)^2+(y_D-y_A)^2}}[(y_D-y_A),-(x_D-x_A)] = \\ &= \frac{F_1}{\sqrt{(\sin\alpha_1)^2+(\cos\alpha_1\sin\beta_1)^2}}[\cos\alpha_1\sin\beta_1,-\sin\alpha_1]\end{aligned}$$

$$\|\mathcal{F}_1\| = |F_1|\sqrt{\frac{(\cos\alpha_1\sin\beta_1)^2}{(\sin\alpha_1)^2+(\cos\alpha_1\sin\beta_1)^2}+\frac{(\sin\alpha_1)^2}{(\sin\alpha_1)^2+(\cos\alpha_1\sin\beta_1)^2}} = |F_1| \quad .$$

Similarly $\mathcal{F}_2$ can be calculated. Using virtual work one may obtain excitation for each variable, which is presented in **paper A**. If $\mathcal{F}_1$ and $\mathcal{F}_2$ have a positive sign than the pendula rotate in anticlockwise direction. Otherwise, the pendula rotate in clockwise direction. Due to symmetry of the system, anticlockwise and clockwise direction derives equal results - CO. If $\mathcal{F}_1$ and $\mathcal{F}_2$ have different sign than CU can be noticed. Let us assume that $\mathcal{F}_1$ has always positive sign and $|F_1| = |F_2| = 0.0206[N]$ (same as in the real system). Depending on the $\mathcal{F}_2$ sign and the initial conditions following the periodic solution can be acquired:

1. the pendula and the beam rotate in the same direction, no phase shift is observed, pendula are in complete synchronization (it corresponds to II normal mode, see Fig 3.4.1);

2. the pendula and the beam rotate in the same direction, π phase (practice) synchronization is observed (it corresponds to I normal mode, see Fig 3.4.2);

3. the pendula rotate in the opposite direction, the beam's ends follow their respective pendula, π anti-phase (practice) synchronization is observed (see Fig 3.4.3);

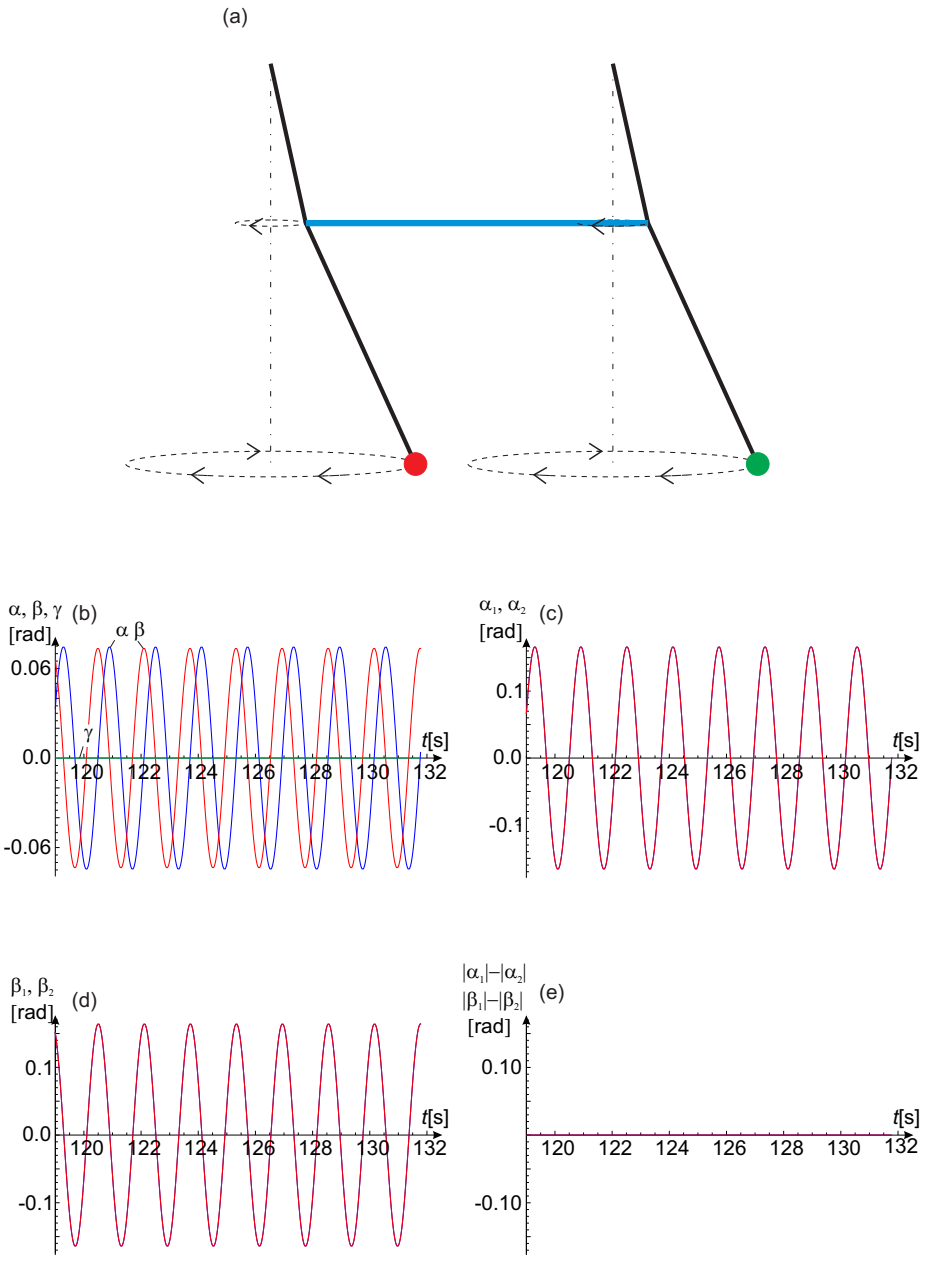

Figure 3.4.1: (a) Shape of 1. periodic solution (b)–(d) time series of complete synchronization for solution number 1; (e) error of synchronization.

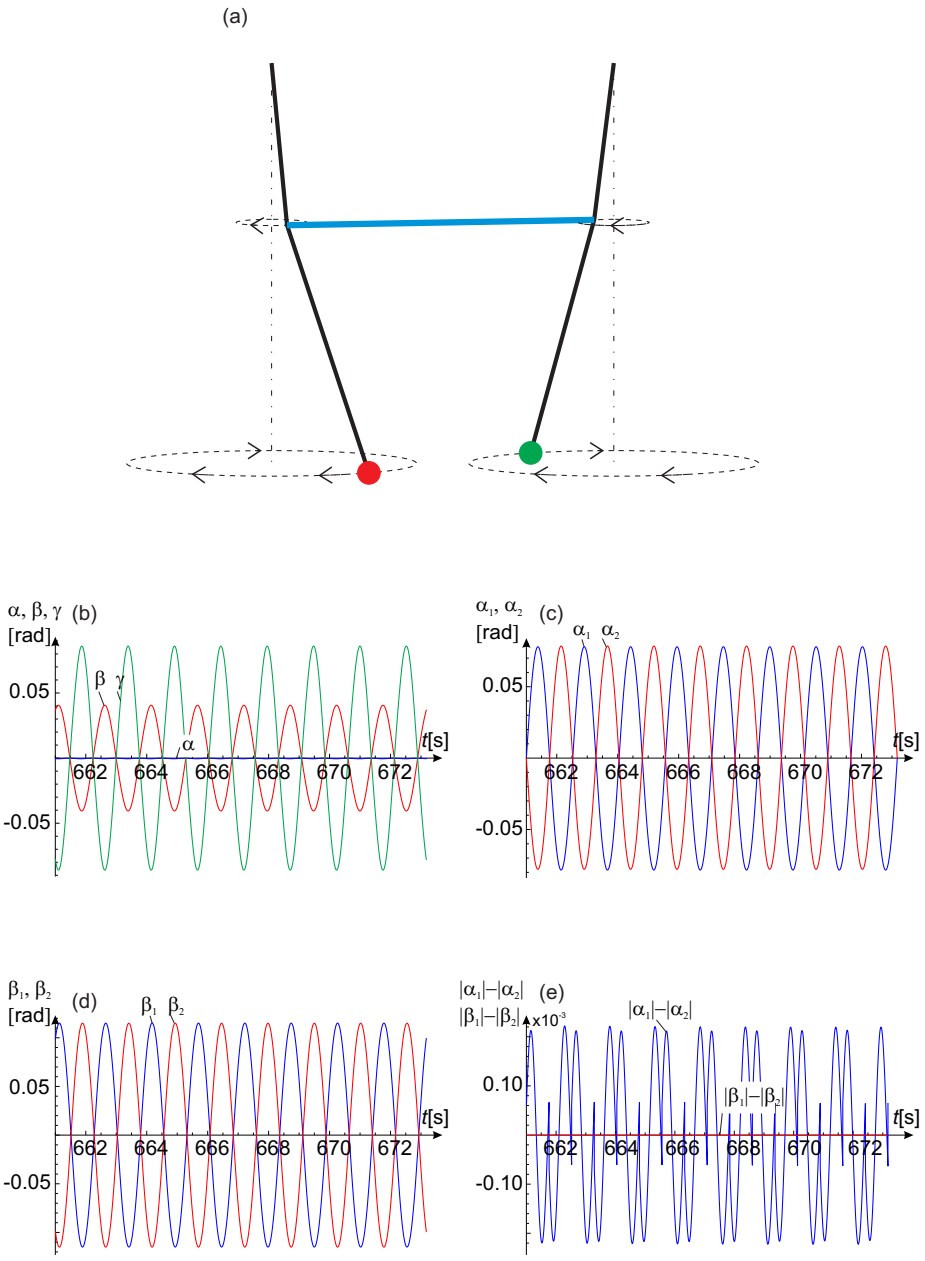

Figure 3.4.2: (a) Shape of 2. periodic solution (b)–(d) time series of almost complete (practical) synchronization for solution number 2; (e) error of synchronization.

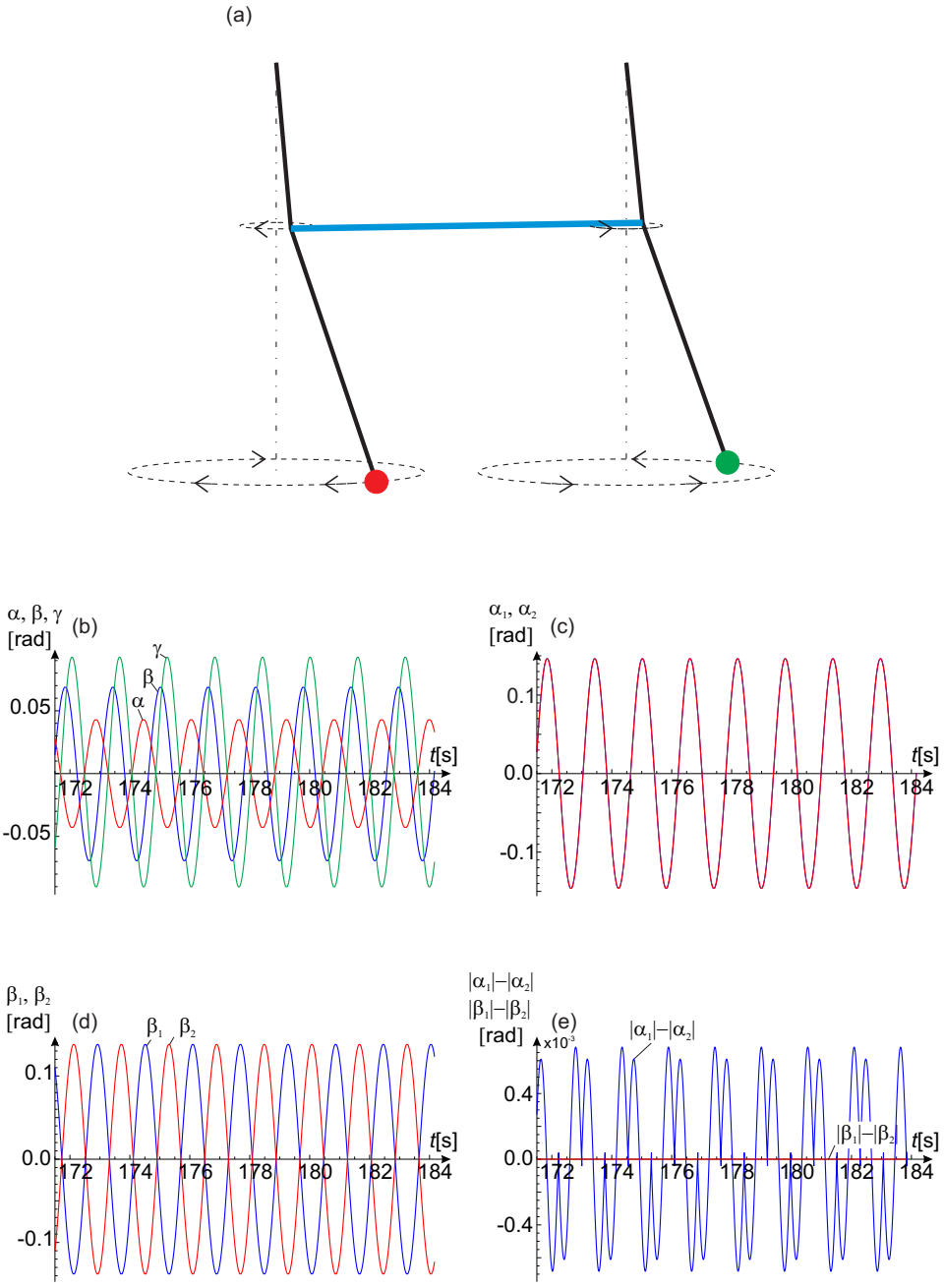

Figure 3.4.3: (a) Shape of 3. periodic solution (b)–(d) time series of almost π anti-phase synchronization for solution number 3; (e) error of synchronization.

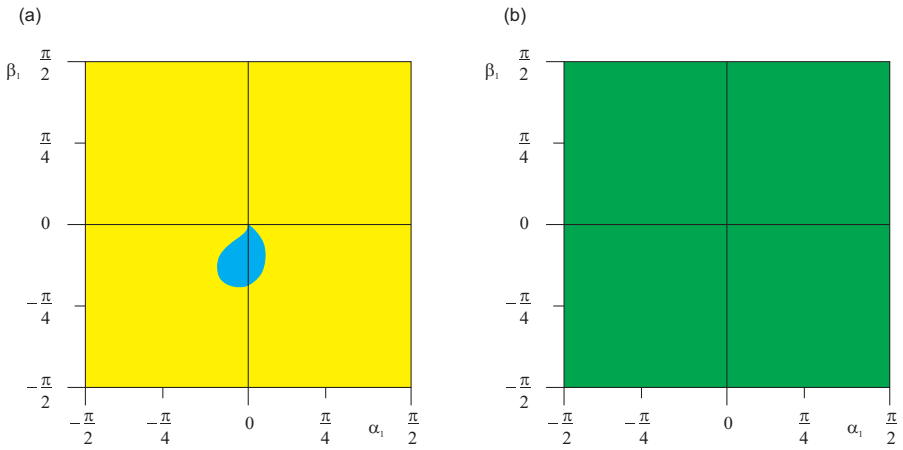

Figure 3.4.4: (a) basins of attraction of different types of synchronization in α_1–β_1 plane: complete synchronization (yellow), π phase synchronization (blue); (b) basins of attraction of π anti-phase synchronization (green) in α_1–β_1 plane.

In our numerical simulations we consider the following parameter values: pendula' masses $m = 0.096$ [kg], the length of the pendula $h = 0.5$ [m], $g = 9.81$ [m s^{-2}] is an acceleration due to the gravity, beam mass $M = 0.5289$ [kg], the length of the beam $b = 1.0$ [m], the beam's string length $l = 0.35$ [m], damping coefficients $c_f = 0.01\sqrt{gh} \approx 0.0221$ [N s m], force $F_1 = F_2 = 0.0206$ [N].

In Fig 3.4.4(a) basins of attraction in α_1–β_1 plane of 1. and 2. CO periodic solution is presented. The following ICs have been taken:$\alpha(0) = 0.0$, $\dot{\alpha}(0) = 0.0$, $\beta(0) = 0.0$, $\dot{\beta}(0) = 0.0$, $\alpha_2(0) = 0.0$, $\dot{\alpha_2}(0) = 0.2$, $\beta_2(0) = 0.2$, $\dot{\beta_2}(0) = 0.0$, $\dot{\alpha}_1(0) = \frac{\dot{\alpha_2}(0)\sin\beta_1}{\sqrt{\cos\alpha_1^2\sin\beta_1^2+\sin\alpha_1^2}}$, $\dot{\beta}_1(0) = \frac{-\dot{\alpha_2}(0)\sin\alpha_1\cos\beta_1}{\sqrt{\cos\alpha_1^2\sin\beta_1^2+\sin\alpha_1^2}}$. The ICs in the presented form guarantee Cartesian initial velocity perpendicular to the pendulum's projection on the XY plane.

In Fig 3.4.4(b) the basins of attraction in α_1–β_1 plane of 3. CU periodic solution is presented. The ICs have been taken in the same way as previously but $F_2 =$ - 0.0206 [N]. There is no other solution for presented parameters and ICs.

If the beam's strings length is changed, then new CU solutions occur. Let us take same ICs and parameter value as in 3. periodic solution. Then let us increase the beam's strings length.

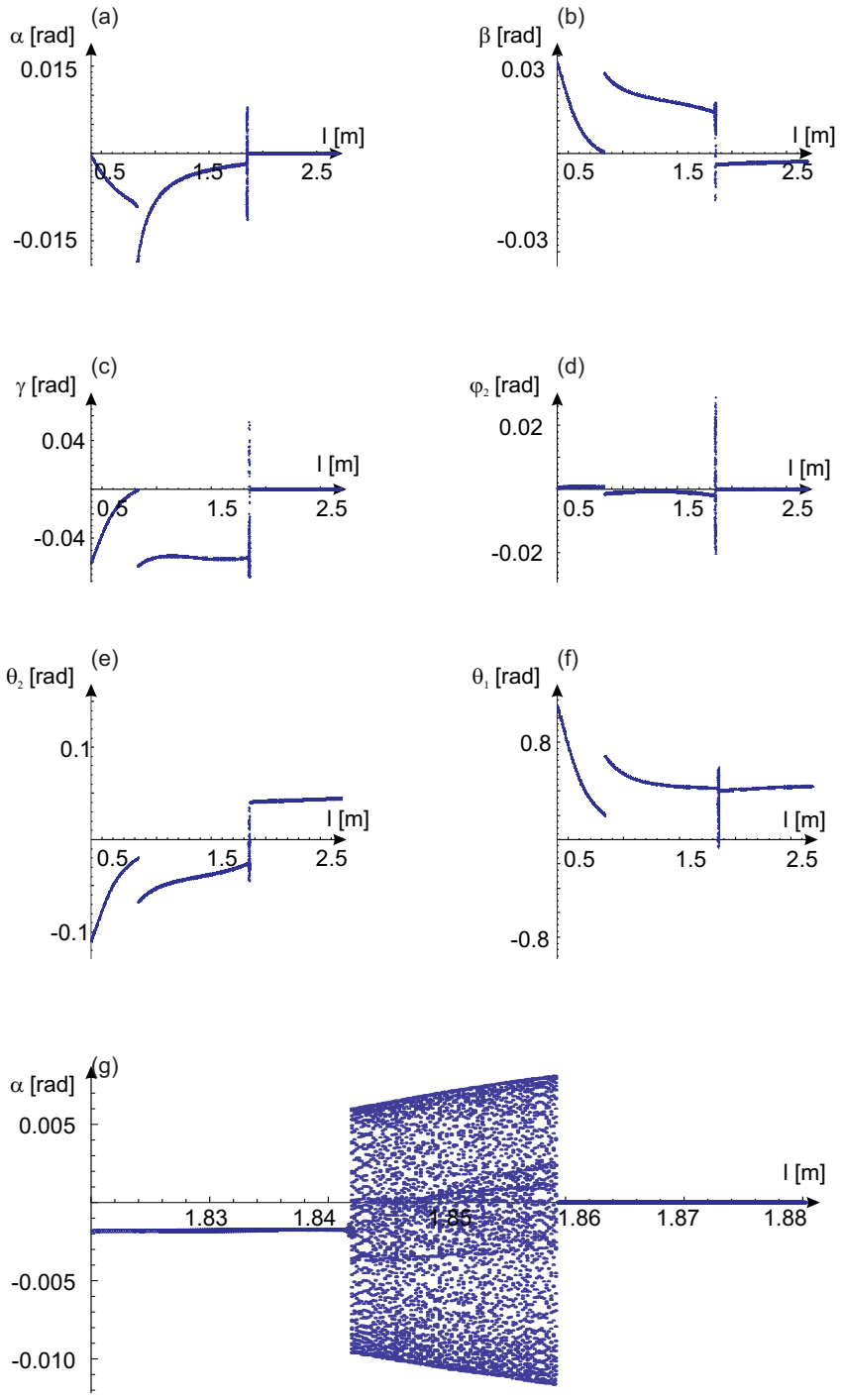

Figure 3.4.5: (a)-(f) bifurcation diagram of beam's strings length l versus: α, β, γ, φ_2, θ_2, θ_1; (g) enlargement of (a) in the set of length l of chaotic solution.

According to the bifurcation diagram in Fig 3.4.5 the received solutions depend on beam's strings length l as follow:

1. for $l \in [0.350, 0.835)$
   - 3. periodic solution;
   - the second pendulum crosses "zero" earlier - there is more than πanti-phase synchronization;
   - the beam rotates around its center of mass (the third variable is a set in motion);
2. for $l \in [0.835, 1.842)$:
   - 3. periodic solution;
   - second pendulum crosses "zero" later - there is less than πanti-phase synchronization;
   - the beam still rotates around its center of mass (the third variable is set in motion);
3. for $l \in [1.842, 1.860)$ there is chaotic motion;
4. for $l \in [1.860, 2.5]$:
   - new periodic solution (see Fig 3.4.6);
   - the second pendulum crosses "zero" in the same time as the first one - there is π anti-phase (complete) synchronization;
   - the beam does not rotate around its center of mass, it swings only in one plane;

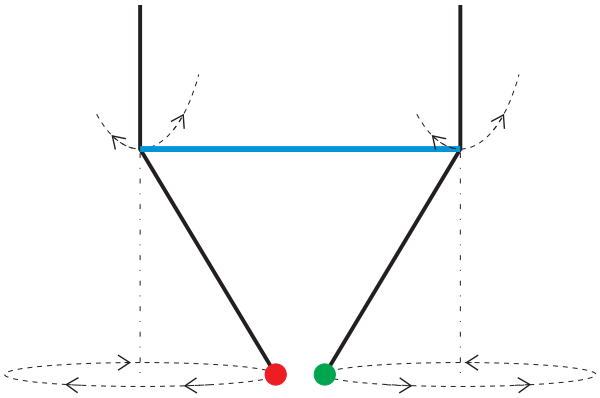

Figure 3.4.6: Shape of new counter rotating periodic solution.

3.4.2 Harmonic excitation

Harmonic excitation usually causes complete synchronization in 2D plane systems and the oscillator's period is the same as the period of excitation (or multiple). In the resonance diagram one may obtain eigenfrequency. Let us consider harmonic excitation in spherical pendulum (3D system). We are interested only in rotational motion . The considered force has to be perpendicular to the pendulum's projection on the XY plane. Let us assume ω as the excitation's frequency. The force is described by the following formula:

$$\mathcal{F} = [F\cos(\omega t), F\sin(\omega t)] \quad .$$

To obtain the excitation for each variable let us consider virtual work introduced for each force:

$$\begin{aligned}
&\partial L = \mathcal{F}_x \partial(x_D - x_A) + \mathcal{F}_y \partial(y_D - y_A) = \\
&= Fh\left(\cos(\omega t)\partial\sin\alpha_1 + \sin(\omega t)\partial\cos\alpha_1\sin\beta_1\right) = \\
&= Fh\left(\left(\cos(\omega t)\cos\alpha_1 - \sin(\omega t)\sin\alpha_1\sin\beta_1\right)\partial\alpha_1 + \sin(\omega t)\cos\alpha_1\cos\beta_1\partial\beta_1\right)
\end{aligned}$$

Force acting on the second pendula can be derived in the same way.

In Fig 3.4.7 two-dimensional resonance diagram is presented. One parameter is the frequency and the second one is the amplitude of excitation.

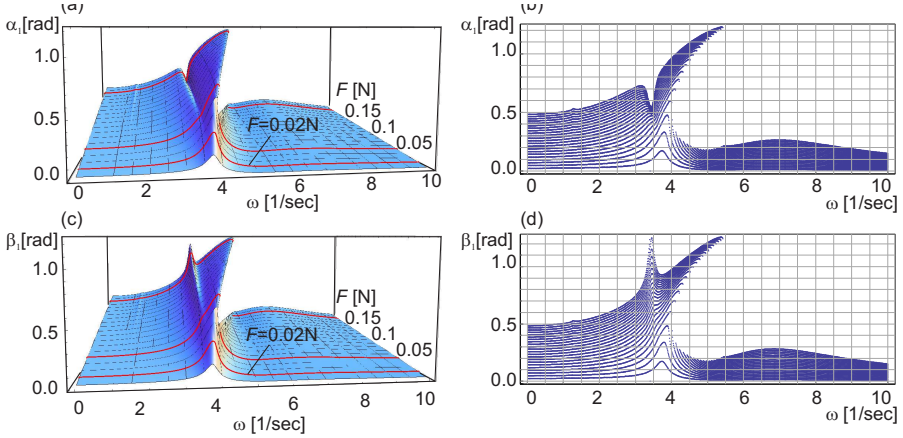

Figure 3.4.7: Two parameter resonance diagram. At axis X the frequency ω of force, at axis Y the amplitude F of force, at axis Z the amplitude of: (a) and (b) α_1; (c) and (d) β_1

The resonance occurs near $\omega = 3.74$ [1/s]. Next, when the amplitude of excitation increases, then the eigenfrequency also increases. Higher excitation

amplitude can by identified with higher total energy in the system. The same effect has been shown in nonlinear normal modes (**paper B**). For higher excitation amplitude, the frequency change causes a rapid damping of the pendulum's amplitude. After $F = 0.06$ [N] the new frequency appears near the resonant one. It induces the symmetry breaking in the pendulum's trajectory. In Fig 3.4.7 (d) there is a characteristic peak near $\omega = 3.47$ [1/s] and for the same value in Fig (b) there is a "cavity". It means that the pendulum's trajectory is no longer a circle but an ellipse. In all studied parameters' area the pendula have been completely synchronized.

In Fig 3.4.8 two dimensional resonance diagram is presented. One parameter is the frequency and the second one is the beam's strings length l. The amplitude of excitation is constant ($F = 0.0206$ [N] - the same as the constant force in real system). One-dimensional resonance diagram is marked in a red line. If the string's length increases, then eigenfrequency decreases.

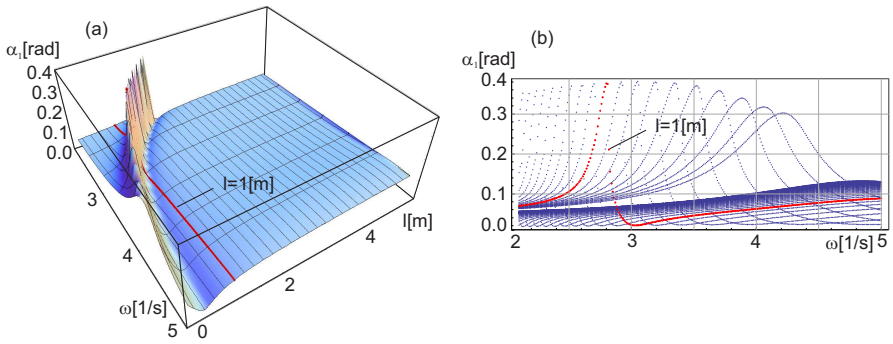

Figure 3.4.8: Two-parameters resonance diagram. At axis X the frequency ω of the force, at axis Y beam's strings length l , at axis Z the amplitude of α_1 .

Also in Fig 3.4.8 an interesting phenomenon is shown: if beam's suspension is longer, then the amplitude death is closer to the resonance frequency. It can explain chaotic oscillation in the bifurcation diagram (Fig 3.4.5) in Section 3.4.1.

3.4.3 Van der Pol excitation

In our studies various excitation types have been considered. Constant force and harmonic excitation are presented. In the dynamical system Van der Pol excitation can be described in the following form [19, 20]:

$$\mathcal{F} = \alpha(q^2 - \mu)\frac{dq}{dt} \quad ,$$

where q is a variable of the system and α, μ are constants. It contains excitation and damping at once. Let us remind that in this study only the rotational motion is considered. If one applies this excitation in all pendula's equations, then the pendula swing only in one plane. It is possible to construct this excitation as follows: let us consider the classical spherical pendulum equation, excitation acts only on the rotational angle, the swing angel be without excitation. Next one can describe the formula of excitation in the changed spherical coordinates (in variables which describe full system). Let us notice that during periodic motion the velocity does not change the sign (will be constant). Thus only the relation between q and μ decides if Van der Pol term is excitation or damping.

Chapter 4

Summary and Conclusions

The aim of this study was to derive a mathematical model of the system, build a physical model of the system, calculate periodic rotational solutions, identify types of synchronization, investigate the influence of initial conditions on the type of synchronization and investigate the influence of different excitations on the type of synchronization.

In **paper A** various mathematical models of the system are presented. The best one is chosen to perform numerical simulations. In the laboratory a real system has been built. The behavior of the real system has been compered with the numerical one. The results proved to be similar to each other.

For the coupled pendula and for the low values of energy (in linear approximation) three rotational modes, each with its own eigenfrequency, have been calculated in **paper B**. To obtain these eigenfrequencies, the theory of linear normal modes has been applied. Next, biased on Newton-Raphson algorithm, the obtained solutions have been continued for larger amplitudes. As one may expect, with increasing total energy level the eigenfrequencies also increase. In the first mode a pitchfork bifurcation has been observed. It has caused the occurrence of new stable periodic solution.

A small perturbation of periodic initial conditions leads to the exchange of energy between the pendula. The energy flows have been shown in **paper B**. Two cases of rotations – in clock-wise and counter clock-wise directions have been considered. In the first case for all three modes we observe the dynamics on a KAM tori. The period of energy transfer is much longer than the natural period of each mode.

In Section 3.4.1 the constant force has been considered. For the parameters' value of the real system numerical simulations have been carried out. Due to them, three periodic solutions have been obtained. In experimental simulations, only two have been gained. The presented basins of attraction show, that different initial conditions cause different types of synchronization. Generally, four types of synchronization have been observed: CS, ICS, PS, APS.

In Section 3.4.2 harmonic excitation has been studied. For high force's amplitude the symmetry breaking of pendulum's trajectory occurred. Also with

growing amplitude of excitation the resonate frequency increases. After the resonance frequency, amplitude of motion has changed rapidly. Next, the change of the beam's suspension causes lower resonate frequency. It can be used to control the system of beam and pendula motion.

Chapter 5

Recommendations for Future Work

The considered system is highly nonlinear. It causes a lot of possible work to be done. Nowadays many researchers investigate the clustering synchronization. It can be interesting to add more spherical pendula to the system and observe possible clusters. Also some parameter mismatch can bring new phenomena. In Section 3.4.3 Van der Pol excitation is introduced. In future work the research on this field should be done.

Within the study of the system the internal resonance has been observed. Moreover, in **paper B** the energy transfer has been briefly considered. A lot of papers presents energy harvesting from pendulum's motion[21, 22].

Each of presented excitation will be closely investigated in the future . In[8, 7, 5] authors, based on 2D pendula, show the analytical method how to obtain synchronous state. It can be difficult to apply this method to the system of spherical pendula, but one may try. Next, the influence of beam's parameter to the pendula's synchronization will be checked. Beam is a coupling. The beam's strings have been examined briefly. What happens if one changes length of the beam?

Bibliography

[1] I. Blekhman, "Synchronization in science and technology," *ASME Press*, New York: 1988.

[2] R. Dilao, "Antiphase and in-phase synchronization of nonlinear oscillators: The huygens's clocks system," *Chaos*, vol. 19, 2009.

[3] K. Czolczynski, P. Perlikowski, A. Stefanski, and T. Kapitaniak, "Why two clocks synchronize: Energy balance of the synchronized clocks," *Chaos: An Interdisciplinary Journal of Nonlinear Science*, vol. 21, no. 2, p. 023129, 2011.

[4] K. Czolczynski, P. Perlikowski, A. Stefanski, and T. Kapitaniak, "Clustering and synchronization of huygens' clocks," *Physica A*, vol. 388, pp. 5013–5023, 2009.

[5] K. Czolczynski, P. Perlikowski, A. Stefanski, and T. Kapitaniak, "Synchronization of pendula rotating in different directions," *Communications in Nonlinear Science and Numerical Simulation*, vol. 17, pp. 3658–3672, 2011.

[6] K. Czolczynski, P. Perlikowski, A. Stefanski, and T. Kapitaniak, "Synchronization of the self-excited pendula suspended on the vertically displacing beam," *Communications in Nonlinear Science and Numerical Simulation*, vol. 18(2), pp. 386–400, 2013.

[7] K. Czolczynski, P. Perlikowski, A. Stefanski, and T. Kapitaniak, "Synchronization of slowly rotating pendulums," *International Journal of Bifurcation and Chaos*, vol. 22, p. 1250128, 2012.

[8] K. Czolczynski, P. Perlikowski, A. Stefanski, and T. Kapitaniak, "Why two clocks synchronize: Energy balance of the synchronized clocks," *Chaos: An Interdisciplinary Journal of Nonlinear Science*, vol. 21, 2011.

[9] P. Brzeski, P. Perlikowski, S. Yanchuk, and T. Kapitaniak, "The dynamics of the pendulum suspended on the forced duffing oscillator," *Journal of Sound and Vibration*, vol. 331, no. 24, pp. 5347 – 5357, 2012.

[10] S. Boda, Z. Neda, B. Tyukodi, and A. Tunyagi, "The rythm of coupled metronomes," *EPJB*, vol. 86, p. 263, 2013.

[11] M. Bennett, M. Schatz, H. Rockwood, and K. Wiesenfeld, "Huygens's clocks," *Proc. R. Soc. Lond. A*, vol. 458, pp. 563–579, 2002.

[12] J. Rubi, A. Rubio, and A. Avello, "Swing-up control problem for a self-erecting double inverted pendulum," *Control Theory and Applications, IEE Proceedings*, vol. 149, no. 2, pp. 169–175, 2002.

[13] A. Steindl and H. Troger, "Bifurcations of the equilibrium of a spherical double pendulum at a multiple eigenvalue," in *Bifurcation: Analysis, Algorithms, Applications*, vol. 79 of *ISNM 79: International Series of Numerical Mathematics*, pp. 277–287, Birkhauser Basel, 1987.

[14] T. Lee, M. Leok, and N. H. McClamroch, "Stable manifolds of saddle points for pendulum dynamics on s2 and so(3)," *ArXiv e-prints*, Mar. 2011.

[15] M. G. Olsson, "The precessing spherical pendulum," *American Journal of Physics*, vol. 46(11), pp. 1118–1120, 1978.

[16] M. G. Olsson, "Spherical pendulum revisited," *American Journal of Physics*, vol. 49, pp. 531–534, 1981.

[17] T. Priest and J. Poth, "Teaching physics with coupled pendulums," *The Physics Teacher*, 1982.

[18] G. Kerschen, M. Peeters, J. C. Golinval, and A. FVakakis, "Nonlinear normal modes, part i: A useful framework for the structural dynamicist," *Mechanical Systems and Signal Processing*, vol. 23, no. 1, pp. 170–194, 2009.

[19] A. Syta and G. Litak, "Dynamical response of a van der pol system with an external harmonic excitation and fractional derivative," in *Discontinuity and Complexity in Nonlinear Physical Systems* (J. A. T. Machado, D. Baleanu, and A. C. J. Luo, eds.), vol. 6 of *Nonlinear Systems and Complexity*, pp. 107–112, Springer International Publishing, 2014.

[20] D. Dudkowski, P. Kuzma, and T. Kapitaniak, "Lag synchronization in coupled multistable van der pol-duffing oscillators," *Discrete Dynamics in Nature and Society*, 2014.

[21] A. S. Paula, M. A. Savi, M. Wiercigroch, and E. Pavlovskaia, "Chaos control methods applied to avoid bifurcations in pendulum dynamics," in *IUTAM Symposium on Nonlinear Dynamics for Advanced Technologies and Engineering Design* (M. Wiercigroch and G. Rega, eds.), vol. 32 of *IUTAM Bookseries (closed)*, pp. 387–395, Springer Netherlands, 2013.

[22] S. Lee, Y. Lee, D. Kim, Y. Yang, L. Lin, Z.-H. Lin, W. Hwang, and Z. L. Wang, "Triboelectric nanogenerator for harvesting pendulum oscillation energy," *Nano Energy*, vol. 2, no. 6, pp. 1113 – 1120, 2013.

PAPER A

Eur. Phys. J. Special Topics **223**, 631–648 (2014)

DOI: 10.1140/epjst/e2014-02130-2

THE EUROPEAN PHYSICAL JOURNAL SPECIAL TOPICS

Review

Modeling of the dynamics of two coupled spherical pendula

B. Witkowski[a]

Division of Dynamics, Technical University of Lodz, 90-924 Lodz, Stefanowskiego 1/15, Poland

Received 3 March 2014 / Received in final form 18 March 2014
Published online 28 April 2014

Abstract. We study the dynamics of the system of two spherical pendula mounted to the rigid beam which hang from the unmovable frame. Using Langrange's multipliers the equations of motion have been derived. We identify two synchronous states in which pendula rotate in the same or different directions. The results of numerical simulations have been confirmed in the simple experiment.

1 Introduction

Currently, there is a great number of research on the coupled pendula [1–17]. However most of them are devoted to the planar motion of oscillating [1–17] or rotating pendula [16,17]. Only a few works consider spherical motion of the pendula. Olssen has considered the dynamics of the spherical pendulum [18,19]. For the small pendulum's motion the derived equation of motion has been solved analytically using Lindstedt-Poincare method. In [20] different methods of solving Hamiltonian systems are presented. In the case of spherical pendulum it is advised to use Lagrange multipliers method instead of penalty method. Priest and Poth [21] have studied the dynamics of two spherical pendula mounted to the rigid beam which hang from the unmovable frame as shown in Fig. 1 focusing on the small oscillations along x-axis. In the present paper we consider the dynamics of the system of Fig. 1 but do not restrict ourselves to small oscillations, i.e., we consider large spherical displacements of the pendula. In the modeling we consider Cartesian, Cartesian with two angles and three angles descriptions of the system. In the first two cases the descriptions require more variables than there are degrees of freedom so one has to use Lagrange's multipliers. The bond equation has square functions and it is impossible to obtain one spatial configuration of the system. Only the third case leads to the unequivocal description of the system. In the numerical simulation we identify two synchronous states in which pendula rotate in the same or different directions. The existence of synchronous states has been confirmed in the simple experiment. The paper is organized as follows. The considered model of the coupled spherical pendula is introduced in Sect. 2. Section 3 presents the results of numerical simulations and their experimental confirmation. Finally, we conclude our studies in Sect. 4.

[a] e-mail: witkowskiblazej@gmail.com

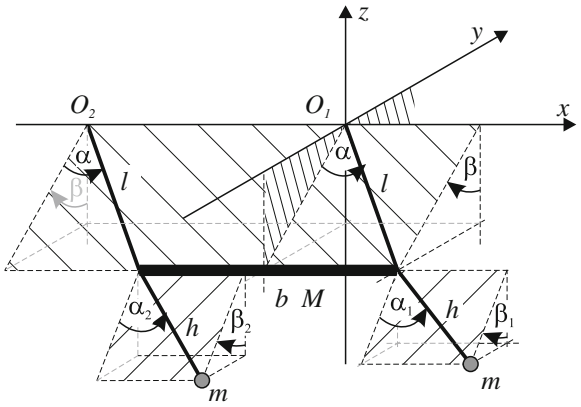

Fig. 1. Model of pendula coupled by a beam.

2 General model for two spherical pendula coupled by the beam

The considered system is composed of a beam and two spherical pendulums as presented in Fig. 1. The beam of mass M is attached to the ends of a weightless and inextensible strings, each of them has length l. At ends of the beam two identical mathematical pendula are suspended, each of length h and mass m.

Model of following system is not straight forward to construct due its complexity. First we introduce separate models of the beam and the pendula. Them we construct the full model of the beam – pendula systems and derive formulas for its kinetic and potential energies. Using these expression one may obtain the second order ODEs describing the motion of the system, from Lagrange equations of the second kind.

2.1 Model of the pendula

2.1.1 Spherical coordinates

The spherical pendulum is typically modeled by two angles φ and θ. The first one describes rotation around z axis, whereas the second one corresponds to inclination from z axis. Then cartesian coordinates have the following form: $x_A = h\cos\varphi\sin\theta$, $y_A = h\sin\varphi\sin\theta$, $z_A = -h\cos\theta$. Kinetic and potential energies are given by:

$$E_k = \tfrac{1}{2}m(\dot{x}_A^2 + \dot{y}_A^2 + \dot{z}_A^2) = \tfrac{1}{2}mh^2(\sin^2\theta\dot{\varphi}^2 + \dot{\theta}^2),$$
$$E_p = mgh(1-\cos\theta).$$

Based on Lagrange equation of the second type one can derive two coupled ODEs of second order (equations of motion). Mass moment of inertia of φ depends on $\sin\theta$. If θ is equal to 0 or π, then mass moment of inertia is equal to 0. Hence equation of motion including φ terms vanishes. These points are also equilibrium points. During motion of the pendulum, while reaching the equilibrium i.e. at the point $\theta = 0$ and its neighbourhood the mass moment of inertia is equal to zero, hence numerical integration of this system is impossible.

2.1.2 Fixed spherical coordinates

To solve the problem of a singular point in the equilibrum point, we change coordinate system to fixed spherical coordinates [22]. Angle β describes rotation about axis x and

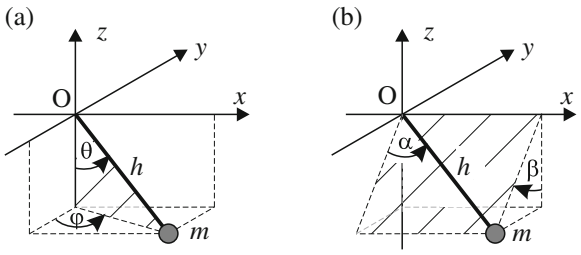

Fig. 2. Pendulum described by: (a) spherical coordinates, (b) fixed spherical coordinates.

angle α is between pendulum and YZ plane, as shown in Fig. 2. The cartesian coordinates are described as follow: $x_A = h\sin\alpha$, $y_A = h\cos\alpha\sin\beta$, $z_A = -h\cos\alpha\cos\beta$ and the kinetic energy is given in the following form:

$$E_k = \tfrac{1}{2}mh^2(\cos^2\alpha\dot{\beta}^2 + \dot{\alpha}^2),$$
$$E_p = mgh(1 - \cos\alpha\cos\beta).$$

The singular point is for $\alpha = -\frac{\pi}{2}$ or $\alpha = \frac{\pi}{2}$. As long as $\alpha < \frac{\pi}{2}$ numerical integration is possible.

2.2 Model of the beam

Solid beam can be considered as a system of 3 points with mass distributed in the following manner: $\frac{1}{6}$ at the ends and $\frac{2}{3}$ in the middle [23]. Let us consider velocity of each point in the following form: $V_A^2 = \dot{x}_A^2 + \dot{y}_A^2 + \dot{z}_A^2, V_B^2 = \dot{x}_B^2 + \dot{y}_B^2 + \dot{z}_B^2, V_C^2 = \dot{x}_C^2 + \dot{y}_C^2 + \dot{z}_C^2$.

2.2.1 Cartesian description

Let us assume, that the motion of each end of the beam is described by 3 Cartesian coordinates: $x_A = x_1$, $y = y_1$, $z_A = z_1$, $x_B = x_2$, $y_B = y_2$, $z_B = z_2$. Coordinates of the center of beam are the average of end-point coordinates of the beam: $x_C = \frac{1}{2}(x_1 + x_2)$, $y_C = \frac{1}{2}(y_1 + y_2)$, $z_C = \frac{1}{2}(z_1 + z_2)$. Kinetic and potential energies of the beam are as follows:

$$\begin{aligned} E_k &= \tfrac{1}{2}M\left(\tfrac{1}{6}V_A^2 + \tfrac{2}{3}V_C^2 + \tfrac{1}{6}V_B^2\right) \\ &= \tfrac{1}{6}M(\dot{x}_1^2 + \dot{y}_1^2 + \dot{z}_1^2 + \dot{x}_1\dot{x}_2 + \dot{y}_1\dot{y}_2 + \dot{z}_1\dot{z}_2 + \dot{x}_2^2 + \dot{y}_2^2 + \dot{z}_2^2), \\ E_p &= Mg\frac{z_1 + z_2}{2}. \end{aligned}$$

The system has 3 degrees of freedom, resulting in 6 variables $(x_1, y_1, z_1, x_2, y_2, z_2)$, so 3 of 6 variables are dependent. Relations between variables are described by the following bond equations:

$$f_1(x_1, y_1, z_1) = \left(x_1 - \tfrac{1}{2}b\right)^2 + y_1^2 + z_1^2 - l^2 = 0,$$
$$f_2(x_2, y_2, z_2) = \left(x_2 + \tfrac{1}{2}b\right)^2 + y_2^2 + z_2^2 - l^2 = 0,$$
$$f_3(x_1, y_1, z_1, x_2, y_2, z_2) = (x_1 - x_2)^2 + (y_1 - y_2)^2 + (z_1 - z_2)^2 - b^2 = 0.$$

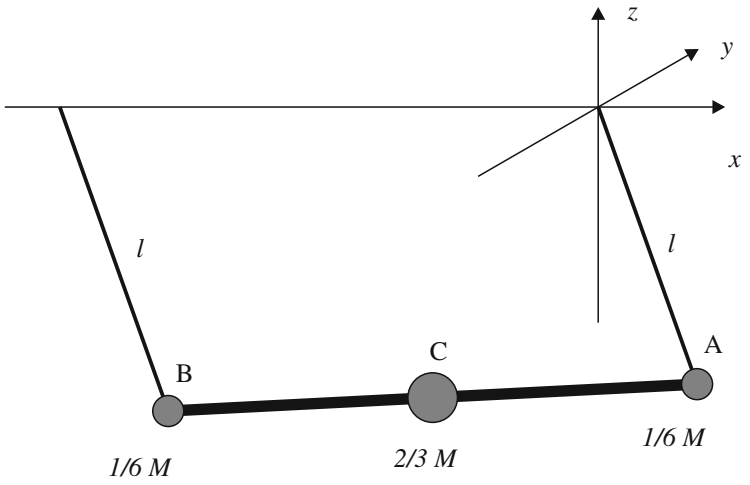

Fig. 3. Beam with mass M described by mass concentrated in 3 points.

Introducing bond equations into equations of motions and using Lagrangea's multipliers, it is possible to define the relations between dependent variables:

$$\frac{d}{dt}\left(\frac{\partial(E_k - E_p)}{\partial \dot{q}_i}\right) - \frac{\partial(E_k - E_p)}{\partial q_i} - \lambda_1 \frac{\partial f_1}{\partial q_i} - \lambda_2 \frac{\partial f_2}{\partial q_i} - \lambda_3 \frac{\partial f_3}{\partial q_i} = 0,$$

where: $i \in \{1, 2, 3, 4, 5, 6\}$ and $q = (x_1, y_1, z_1, x_2, y_2, z_2)$. There exist two values of each depending variables, since bond equations are square. As the consequence, numerical integration is ambigious, since it is unknown which solution has to be chosen.

2.2.2 Cartesian description with two angles

Geometry of the system is described by the following coordinates: x, y, z, and 2 angles φ, θ. Point C is a center of beam, points A and B are at the ends of the beam given by the formulas: $x_A = \frac{1}{2}b\cos\varphi\cos\theta + x$, $y_A = \frac{1}{2}b\sin\varphi\cos\theta + y$, $z_A = \frac{1}{2}b\sin\theta + z$, $x_B = -\frac{1}{2}b\cos\varphi\cos\theta + x$, $y_B = -\frac{1}{2}b\sin\varphi\cos\theta + y$, $z_B = -\frac{1}{2}b\sin\theta + z$. One obtains more variables than degrees of freedom of the system.

$$f_1(\varphi, \theta, x_0, y_0, z_0) = \left(x_A - \tfrac{1}{2}b\right)^2 + y_A^2 + z_A^2 - l^2 = 0,$$
$$f_2(\varphi, \theta, x_0, y_0, z_0) = \left(x_B + \tfrac{1}{2}b\right))^2 + y_B^2 + z_B^2 - l^2 = 0.$$

Kinetic and potential energy are given by formulas:

$$E_k = \tfrac{1}{2}M\left(\tfrac{1}{6}V_A^2 + \tfrac{2}{3}V_C^2 + \tfrac{1}{6}V_B^2\right) = \tfrac{1}{2}M(\dot{x}^2 + \dot{y}^2 + \dot{z}^2 + \tfrac{1}{12}b(\cos^2\theta\dot{\varphi}^2 + \dot{\theta}^2)),$$
$$E_p = Mgz.$$

To find dependent variables, Lagrangea's multipliers method is used. The second order ODEs of the system can be obtained from modified second Lagrange equation:

$$\frac{d}{dt}\left(\frac{\partial Lag}{\partial \dot{q}_i}\right) - \frac{\partial Lag}{\partial q_i} - \lambda_1 \frac{\partial f_1}{\partial q_i} - \lambda_2 \frac{\partial f_2}{\partial q_i} = 0 \quad i \in \{1, 2, 3, 4, 5\},$$

$$q = (\varphi, \theta, x_0, y_0, z_0).$$

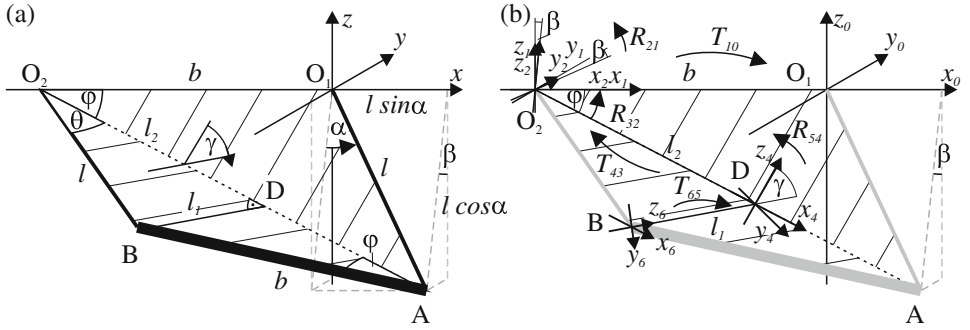

Fig. 4. Beam, which position is described by 3 angles.

There exist two values of each depending variables, since bond equations are square. As the consequence, numerical integration is ambigious, since it is unknown which solution has to be chosen, similarly as in Sect. 2.2.1

2.2.3 Three angles' desription

In this section, motion of the beam is describe using three independent variables. Cartesian coordinates of first beam's end A can be obtained by angles: α and β, like in spherical pendulum. Third variable is is given by the following geometric construction: draw a line from point O_2 to point A, the space between beam and strings is divided to 2 triangles: $\triangle BO_2A$ and $\triangle O_1O_2A$ (Figure 4). The angle γ, between those triangles, describes unequivocally position of point B.

To fully describe the motion of the beam, Cartesian coordinates of points: A, B and C have to be known. Point A is described by angles α and β. Coordinates of point C are the average of the coordinates of point A and B. To obtain point B one has to add auxiliary variables.

Let us mark line segment $\overline{O_2A}$ as d. Basing on cosine theorem, one obtains: $d^2 = l^2 + b^2 - 2lb\cos(\alpha + \frac{\pi}{2}) = l^2 + b^2 + 2lb\sin\alpha$. Marking angle $\angle O_1O_2A$ as φ, $\sin\varphi = \frac{l\cos\alpha}{d}$, $\cos\varphi = \frac{b+l\sin\alpha}{d}$ and $\angle O_1AO_2$ as θ, then using sine theorem for $\triangle O_1O_2A$ one receives: $\frac{l}{\sin\varphi} = \frac{b}{\sin\theta}$, $\sin\theta = \frac{b\sin\varphi}{l} = \frac{b\cos\alpha}{d}$. From cosine theorem $\cos\theta$ can be obtained: $\cos\theta = \frac{b^2-l^2-d^2}{-2ld} = \frac{l+b\sin\alpha}{d}$. Due to the similarity between triangles $\triangle O_1O_2A$ and $\triangle ABO_2$ we have the following relations between angles: $\angle O_1O_2A$ is equal to $\angle O_2AB$, $\angle O_1AO_2$ is equal to $\angle AO_2B$. The height l_1 of triangle $\triangle ABO_2$ is given by $l_1 = l\sin\theta = \frac{bl\cos\alpha}{d}$ and it crosses $\overline{O_2A}$ at point D. Denoting $\overline{O_2D}$ as l_2, we have $l_2 = l\cos\theta = \frac{l^2+bl\sin\alpha}{d}$.

Several transformations of local B coordinate system have to be performed as in Fig. 4, in order to obtain Cartesian coordinates of point B corresponding to main coordinate system. Let us consider B coordinate system as follow: x axis is parallel to d, y axis is perpendicular to d and center of this system is in point B. First, the translation of the system from point B to point D by l_1 about z_6 axis is performed. In the next step, rotation of system by θ about x_5 axis takes place. Then, translation from point D to point O_2 by l_2 along x_4 axis occurs. Furthermore, one rotates system by φ about y_3 axis and by β about x_2 axis. Eventually, translation of the system from point O_2 to point O_1 by b along x_1 axis is performed. Each step is described by the

following matrices:

$$T_{65} = \begin{bmatrix} 1 & 0 & 0 & -l_1 \\ 0 & 1 & 0 & 0 \\ 0 & 0 & 1 & 0 \\ 0 & 0 & 0 & 1 \end{bmatrix}, \quad T_{43} = \begin{bmatrix} 1 & 0 & 0 & l_2 \\ 0 & 1 & 0 & 0 \\ 0 & 0 & 1 & 0 \\ 0 & 0 & 0 & 1 \end{bmatrix}, \quad T_{10} = \begin{bmatrix} 1 & 0 & 0 & -b \\ 0 & 1 & 0 & 0 \\ 0 & 0 & 1 & 0 \\ 0 & 0 & 0 & 1 \end{bmatrix},$$

$$R_{45} = \begin{bmatrix} 1 & 0 & 0 & 0 \\ 0 & \cos\gamma & -\sin\gamma & 0 \\ 0 & \sin\gamma & \cos\gamma & 0 \\ 0 & 0 & 0 & 1 \end{bmatrix}, \quad R_{32} = \begin{bmatrix} \cos\varphi & 0 & \sin\varphi & 0 \\ 0 & 1 & 0 & 0 \\ -\sin\varphi & 0 & \cos\varphi & 0 \\ 0 & 0 & 0 & 1 \end{bmatrix},$$

$$R_{21} = \begin{bmatrix} 1 & 0 & 0 & 0 \\ 0 & \cos\beta & -\sin\beta & 0 \\ 0 & \sin\beta & \cos\beta & 0 \\ 0 & 0 & 0 & 1 \end{bmatrix}.$$

Finally, coordinates of point B are as follows:

$$\begin{bmatrix} x_B \\ y_B \\ z_B \\ 1 \end{bmatrix} = T_{10}R_{21}R_{32}T_{43}R_{54}T_{65} \begin{bmatrix} 0 \\ 0 \\ 0 \\ 1 \end{bmatrix}.$$

After calculations, the above matrix takes the following form:

$$x_B = \frac{l(b + l\sin\alpha)(l + b\sin\alpha)}{d^2} - \frac{l^2 b\cos\alpha^2\cos\gamma}{d^2} - b,$$

$$y_B = \frac{l\cos\alpha(\sin\beta(b\cos\gamma(b + l\sin\alpha) + l(l + b\sin\alpha)) + d\,b\cos\beta\sin\gamma)}{d^2},$$

$$z_B = -\frac{l\cos\alpha(\cos\beta(b\cos\gamma(b + l\sin\alpha) + l(l + b\sin\alpha)) - d\,b\sin\beta\sin\gamma)}{d^2}.$$

Finally the following formulas:

$$E_k = \tfrac{1}{2}M\left(\tfrac{1}{6}V_A^2 + \tfrac{2}{3}V_C^2 + \tfrac{1}{6}V_B^2\right),$$
$$E_p = Mgz_C,$$

describe kinetic and potential energies of the beam.

2.3 Complete system

Let us consider the full system composed of a beam and two spherical pendula. The beam is described by model with 3 angles (as in Sect. 2.2.3) and the pendula are described by fixed spherical coordinates as follow:

$$x_D = h\sin\alpha_1 + x_A,\ y_D = h\cos\alpha_1\sin\beta_1 + y_A,\ z_D = -h\cos\alpha_1\cos\beta_1 + z_A,$$
$$x_E = h\sin\alpha_2 + x_B,\ y_E = h\cos\alpha_2\sin\beta_2 + y_B,\ z_E = -h\cos\alpha_2\cos\beta_2 + z_B.$$

Kinetic energy and potencial energy is given by formulas:

$$E_k = \tfrac{1}{2}\left(M\left(\tfrac{1}{6}V_A^2 + \tfrac{2}{3}V_C^2 + \tfrac{1}{6}V_B^2\right) + m\left(V_D^2 + V_E^2\right)\right),$$
$$E_p = Mgz_C + mg\left(z_D + z_E\right),$$
$$Lag = E_k - E_p.$$

Viscous damping is assumed. Variable γ describes motion of the beam around fictional axis (diagonal between point A and O_2). Damping for this variable should correspond to damping in node O_2. Let us consider new variables α^*, β^* in point B, derived similarly as for point A:

$$\begin{aligned} x_B &= \frac{l(b + l\sin\alpha)(l + b\sin\alpha)}{d^2} - \frac{l^2 b\cos\alpha^2\cos\gamma}{d^2} - b \\ &\equiv l\sin\alpha^* - b, \\ y_B &= \frac{l\cos\alpha(\sin\beta(b\cos\gamma(b + l\sin\alpha) + l(l + b\sin\alpha)) + d\,b\cos\beta\sin\gamma)}{d^2} \\ &\equiv l\cos\alpha^*\sin\beta^*, \\ z_B &= -\frac{l\cos\alpha(\cos\beta(b\cos\gamma(b + l\sin\alpha) + l(l + b\sin\alpha)) - d\,b\sin\beta\sin\gamma)}{d^2} \\ &\equiv -l\cos\alpha^*\cos\beta^*. \end{aligned}$$

Then:

$$\alpha^* = \arcsin\left(\frac{(b + l\sin\alpha)(l + b\sin\alpha) - lb\cos\alpha^2\cos\gamma}{d^2}\right),$$
$$\beta^* = \arctan\left(\frac{\sin\beta(b\cos\theta(b + l\sin\alpha) + l(l + b\sin\alpha)) + d\,b\cos\beta\sin\gamma}{\cos\beta(b\cos\theta(b + l\sin\alpha) + l(l + b\sin\alpha)) - d\,b\sin\beta\sin\gamma}\right).$$

After obtaining derivative $\dot\alpha^*$ and $\dot\beta^*$, damping function takes the following form:

$$\begin{aligned} R(q,\dot q) = \ & \tfrac{1}{2}C_f\left(\dot\alpha^2 + \dot\beta^2 + \dot\alpha^{*2} + \dot\beta^{*2}\left(\cos\left(\beta - \beta_1\right)\dot\alpha - \dot\alpha_1\right)^2 + \right. \\ & \left.\left(\dot\beta - \dot\beta_1\right)^2 + \left(\cos\left(\beta^* - \beta_2\right)\dot\alpha^* - \dot\alpha_2\right)^2 + \left(\dot\beta^* - \dot\beta_1\right)^2\right). \end{aligned}$$

Let us consider pendula's excitation as constant forces F_1 and F_2. Those forces are prependicular to pendulum's projection on plane XY. The formula describing the excitation force can be found in Appendix A.

$$\begin{aligned} \mathcal{F}_1 &= \frac{F_1}{\sqrt{(x_D - x_A)^2 + (y_D - y_A)^2}}\left[y_D - y_A, -(x_D - x_A)\right] \\ &= \frac{F_1}{\sqrt{(\sin[\alpha_1])^2 + (\cos[\alpha_1]\sin[\beta_1])^2}}\left[\cos\alpha_1\sin\beta_1, -\sin\alpha_1\right], \\ \mathcal{F}_2 &= \frac{F_2}{\sqrt{(\sin\alpha_2)^2 + (\cos\alpha_2\sin\beta_2)^2}}\left[\cos\alpha_2\sin\beta_2, -\sin\alpha_2\right]. \end{aligned}$$

Based on Lagrange equation of second type one can derive seven coupled second ODEs. The equations of the motion of the system are following:

$$\frac{d}{dt}\left(\frac{\partial Lag}{\partial\dot q_i}\right) - \frac{\partial Lag}{\partial q_i} + \frac{\partial R}{\partial\dot q_i} = T_{q_i}, \quad i \in \{1,2,3,4,5,6,7\}, \tag{1}$$

$$q = (\alpha\beta, \gamma, \alpha_1, \beta_1, \alpha_2, \beta_2),$$

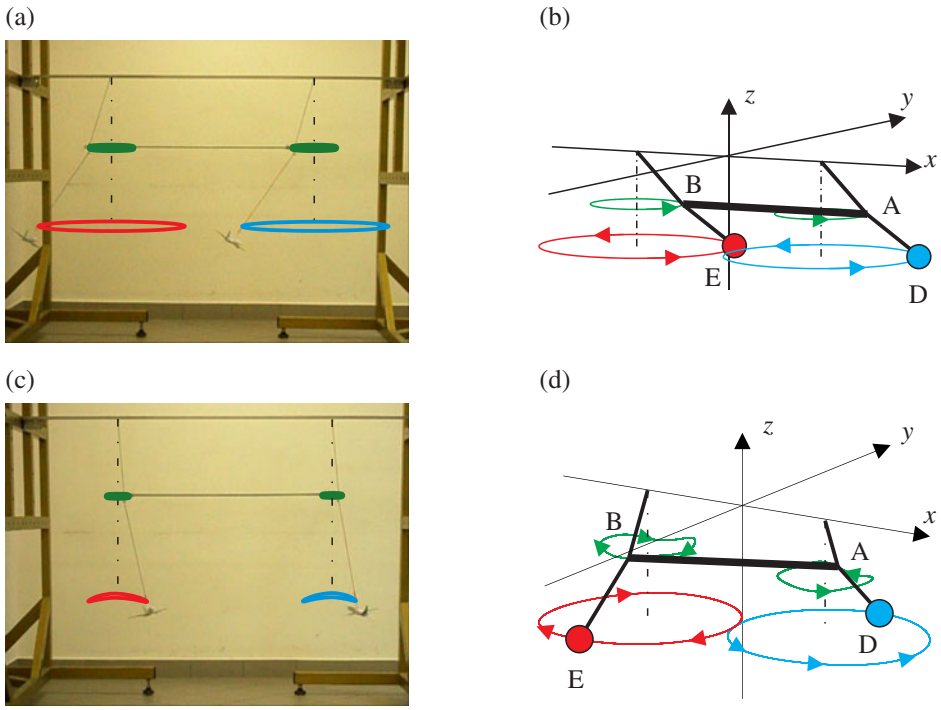

Fig. 5. (a)–(b) Beam's and pendula's rotating motion in the same direction in phase: (a) experimental observation, (b) numerical simulation; (c)–(d) Beam's and pendula's rotating motion in opposite direction in phase with shift π: (c) experimental observation, (d) numerical simulation.

T_{q_i} is external momentum acting on $i-th$ varaiable. The equations of the motion of the system can be found in Appendix B.

3 Experimental observation and numerical simulations

In our simple experiment we consider pendula of the lengths $h = 0.5\,\mathrm{m}$ and masses $m = 0.096\,\mathrm{kg}$ which hang from the beam of the length $b = 1.0\,\mathrm{m}$ and the mass $M = 0.5\,\mathrm{kg}$. The beam hangs from the unmovable base on the massless strings of the length $l = 0.35\,\mathrm{m}$ connected to its ends. To compensate the effect of damping we excite the rotations of the pendula by two 1.5 V DC motors (for better visualization we use toy airplanes manufactured by *Premier Portfolio*).

The system behavior has been video recorded and the beam and pendula's trajectories have been determined using image analysis software *Kinovea*. The video clip describing the synchronous motion of pendula can be found at: `http://team.kdm.p.lodz.pl/movies.html`.

Two types of stable synchronous motion have been identified as shown in Fig. 5a,c. In the first type both pendula synchronize in-phase and rotate in the same direction and we observe in-phase synchronization of the beam and pendula motion (Fig. 5a). In the second type the pendula synchronize in anti-phase and rotate in the opposite directions (Fig. 5c). The performed experiments have not revealed any other stable types of pendula rotating motion.

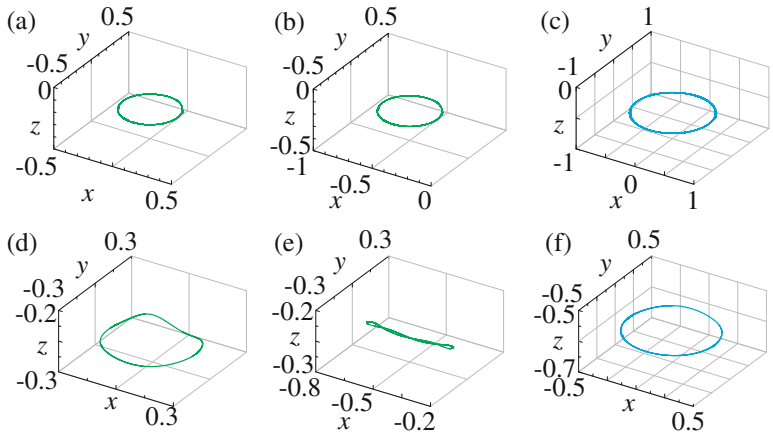

Fig. 6. Trajectory of the beam and the pendulas displacements: $l = 0.35$, $b = 1$, $h = 0.5$, $g = 9.81$, $M = 0.5$, $m = 0.096$, $C_f = 0.01\sqrt{gh}$, $F_1 = 0.0206$, $F_2 = 0.0206$, (a–c) both pendula rotate in the same direction ($\alpha = 0$, $\beta = 0$, $\gamma = 0$, $\alpha_1 = \pi/6$, $\beta_1 = 0$, $\alpha_2 = \pi/5$, $\beta_2 = 0$, $\dot{\alpha} = 0$, $\dot{\beta} = 0$, $\dot{\gamma} = 0$, $\dot{\alpha_1} = 0$, $\dot{\beta_1} = 1$, $\dot{\alpha_2} = 0$, $\dot{\beta_2} = 1.2$); (d–f) both pendula rotate in opposite directions ($\alpha = 0$, $\beta = 0$, $\gamma = 0$, $\alpha_1 = \pi/6$, $\beta_1 = 0$, $\alpha_2 = \pi/5$, $\beta_2 = 0$, $\dot{\alpha} = 0$, $\dot{\beta} = 0$, $\dot{\gamma} = 0$, $\dot{\alpha_1} = 0$, $\dot{\beta_1} = 1$, $\dot{\alpha_2} = 0$, $\dot{\beta_2} = -1.2$).

Our experimental observations have been confirmed in numerical simulations as can be seen in Fig. 5b,d (we use the following parameter values: $M = 0.5\,\text{kg}$, $b = 1\,\text{m}$, $l = 0.35\,\text{m}$, $h = 0.5\,\text{m}$, $m = 0.096\,\text{kg}$). The equations of motion 1 have been integrated using Runge-Kutta-Fehlberg 45 method.

During the first type of synchronous rotating motion both pendula and the beam rotate in the $x - y$ plane (there is no motion along z-axis) as one observes in Fig. 6a–c where the trajectories of the beam's end A, beam's center C and pendulum D have been shown. The second type of synchronous motion is characterized by the small motion along z-axis (Fig. 6d–f) and the trajectories of the beam's end A, beam's center C and pendulum D create three-dimensional closed curves.

4 Summary

We study the dynamics of two spherical pendula mounted to the rigid beam which hang from the unmovable frame. The beam of mass M has been discretized by three masses (two masses $\frac{1}{6}M$ located at the ends of the beam and mass $\frac{2}{3}M$ located at the beam's center). We describe in details the derivation of the unequivocal equations of motion. In the numerical simulations we identify two different types of the synchronous motion of the spherical pendula, i.e., both pendula rotate in the same direction (co-rotating pendula) or the pendula rotate in the opposite direction (counter-rotating pendula). During co-rotating motion the beam does not oscillate around z-axis (it oscillates in the $z - x$ plane). The center of the beam is moving along the three-dimensional closed curve when the pendula counter-rotate. Numerical results have been verified in the simple experiment which allows for the observation of the same types of synchronous motion.

This work has been supported by the Foundation for Polish Science, Team Programme under project TEAM/2010/5/5. BW would like to thank to prof. Kapitaniak and prof. Strzalko for their kind help and suggestions.

Appendix A

Damping function takes the following form:

$$R(q,\dot{q}) = \tfrac{1}{2}C_f(\dot{\alpha}^2 + \dot{\beta}^2 + \dot{\alpha}^{*2} + \dot{\beta}^{*2}(\cos(\beta-\beta_1)\dot{\alpha} - \dot{\alpha_1})^2 + (\dot{\beta}-\dot{\beta}_1)^2 + (\cos(\beta^*-\beta_2)\dot{\alpha}^* - \dot{\alpha_2})^2 + (\dot{\beta}^*-\dot{\beta}_1)^2),$$

where:

$$\dot{\alpha}^* = -4l^2bd'\cos\alpha^2\sin\left(\tfrac{\gamma}{2}\right)^2 + \frac{d\left(\alpha' d^2\cos\alpha + l^2b\left(-2\alpha'\sin 2\alpha\sin\left(\tfrac{\gamma}{2}\right)^2 + \gamma'\cos\alpha^2\sin\gamma\right)\right)}{d\sqrt{d^4 - \left(d^2\sin\alpha + 2l^2b\cos\alpha^2\sin\left(\tfrac{\gamma}{2}\right)^2\right)^2}},$$

$$\dot{\beta}^* = \frac{bQ}{\left(b\cos\gamma\left(b + l\sin\alpha\right) + l\left(l + b\sin\alpha\right)\right)^2 + b^2d^2\sin\gamma^2} + \dot{\beta},$$

where:

$$Q = d'\sin\gamma(b\cos\gamma(b + l\sin\alpha) + l(l + b\sin\alpha)) + d\Big(-4\alpha' lb\cos\alpha\cos\left(\tfrac{\gamma}{2}\right)^3\sin\left(\tfrac{\gamma}{2}\right)^3\sin\tfrac{\gamma}{2} + \gamma'\left(b^2 + l^2\cos\gamma + lb\sin\alpha(1+\cos\gamma)\right)\Big)$$

$$d = \sqrt{l^2 + b^2 + 2lb\sin\alpha}, \quad d' = \frac{lb\alpha'\cos\alpha}{\sqrt{l^2 + b^2 + 2lb\sin\alpha}}.$$

Then damping for each variable is give as:

$$C_q = \frac{\partial R}{\partial\dot{q}},$$

where $q = (\alpha\beta, \gamma, \alpha_1, \beta_1, \alpha_2, \beta_2)$.

We assume that external force is prependicular to pendulum's projection on plane XY:

$$\begin{aligned}\mathcal{F}_1 &= \frac{F_1}{\sqrt{(x_D - x_A)^2 + (y_D - y_A)^2}}\left[y_D - y_A, -(x_D - x_A)\right] \\ &= \frac{F_1}{\sqrt{(\sin\alpha_1^2 + (\cos\alpha_1\sin\beta_1)^2}}\left[\cos\alpha_1\sin\beta_1, -\sin\alpha_1\right]. \\ \mathcal{F}_2 &= \frac{F_2}{\sqrt{(\sin[\alpha_2])^2 + (\cos\alpha_2\sin\beta_2)^2}}\left[\cos\alpha_2\sin\beta_2, -\sin\alpha_2\right].\end{aligned}$$

To obtain excitation for each variable let us consider virtual work introduced for each force:

$$\begin{aligned}\partial L &= F_{1x}\partial(x_D - x_A) + F_{1y}\partial(y_D - y_A) + F_{2x}\partial(x_E - x_B) + F_{2y}\partial(y_E - y_B) \\ &= \frac{F_1 h}{\sqrt{(\sin\alpha_1)^2 + (\cos\alpha_1\sin\beta_1)^2}}\left(\sin\beta_1\partial\alpha_1 - \sin\alpha_1\cos\alpha_1\cos\beta_1\partial\beta_1\right) \\ &\quad + \frac{F_2 h}{\sqrt{(\sin\alpha_2)^2 + (\cos\alpha_2\sin\beta_2)^2}}\left(\sin\beta_2\partial\alpha_2 - \sin\alpha_2\cos\alpha_2\cos\beta_2\partial\beta_2\right),\end{aligned}$$

where $\partial(x_D - x_A)$ and $\partial(y_D - y_A)$ and $\partial(x_E - x_B)$ and $\partial(y_E - y_B)$ are virtual displacments respectively for $\mathcal{F}_1$ and $\mathcal{F}_2$.

Then one obtains:

$$T_{\alpha_1} = F_1 h \frac{\sin\beta_1}{\sqrt{(\sin\alpha_1)^2 + (\cos\alpha_1 \sin\beta_1)^2}},$$

$$T_{\beta_1} = -F_1 h \frac{\sin\alpha_1 \cos\alpha_1 \cos\beta_1}{\sqrt{(\sin\alpha_1)^2 + (\cos\alpha_1 \sin\beta_1)^2}},$$

$$T_{\alpha_2} = F_2 h \frac{\sin\beta_2}{\sqrt{(\sin\alpha_2)^2 + (\cos\alpha_2 \sin\beta_2)^2}},$$

$$T_{\beta_2} = -F_2 h \frac{\sin\alpha_2 \cos\alpha_2 \cos\beta_2}{\sqrt{(\sin\alpha_2)^2 + (\cos\alpha_2 \sin\beta_2)^2}}.$$

We assume that beam has no external excitation: $T_\alpha = 0$, $T_\beta = 0$, $T_\gamma = 0$.

Appendix B

Coupled second order ordinary differential equations, which describe the system of Fig. 1 can by written by matrices of: mass M $7x7$, torque T $7x1$, damping C $7x1$ and rest RR $7x1$:

$$M(q,\dot{q})\ddot{q} + C(q)\dot{q} + RR = T,$$
$$q = (\alpha\beta, \gamma, \alpha_1, \beta_1, \alpha_2, \beta_2),$$

$$\begin{aligned}
M_{11} = {} & \frac{1}{48d^8} l^2 \Big(4d^6(4l^2M - b^2(M-3m)) + 16d^8(M+3m) \\
& -d^2b^2(32l^4 - 55l^2b^2 + 32b^4)(M+3m) + 4b^2(8l^6 + l^4b^2 + l^2b^4 + 8b^6) \\
& \times(M+3m) + 4d^4(4l^4(M+3m) + 2l^2b^2(M+3m) + b^4(7M+9m)) \\
& + b\Big(8b(d^6M - 2d^2l^2b^2(M+3m) + 6l^2b^2(l^2+b^2)(M+3m) \\
& +2d^4l^2(4M+9m))\cos\theta + 4l^2b^3(M+3m)\cos 4\alpha \cos\left(\tfrac{\theta}{2}\right)^2 (4(l^2+b^2) \\
& -11d^2(4(l^2+b^2) - 13d^2)\cos\theta) + b(-4d^6 - 7d^2l^2b^2 + 12l^2b^2(l^2+b^2) \\
& + 4d^4(2l^2+b^2)(M+3m))\cos 2\theta + 4b\cos 2\alpha(-3d^6(M+m) \\
& -d^2(8l^4 - 5l^2b^2 + 8b^4)(M+3m) + 4(2l^6 + l^4b^2 + l^2b^4 + 2b^6)(M+3m) \\
& + d^4(-4l^2(M+3m) + b^2(5M+3m)) - 2(d^6M + 6d^4l^2m + 8d^2l^2b^2(M+3m) \\
& -8l^2b^2(l^2+b^2)(M+3m))\cos\theta + (d^6 - (d^4 + 5d^2l^2 - 4l^4)b^2 + 4l^2b^4) \\
& \times(M+3m)\cos 2\theta) + 4l(4d^6M + 6d^2b^2(l^2+b^2)(M+3m) \\
& + 2b^2(4l^4 - 5l^2b^2 + 4b^4)(M+3m) + d^4(b^2(M-3m) + 8l^2(M+3m)) \\
& + 2(2d^6M + 4l^2b^4(M+3m) + 4d^2b^2(l^2+b^2)(M+3m) \\
& + d^4(b^2M + 4l^2(M+3m))) + \cos\theta + b^2(d^4 + 2l^2b^2 + 2d^2(l^2+b^2)) \\
& \times(M+3m)\cos(2\theta))\sin\alpha + 4lb^2(6d^2(l^2+b^2)(M+3m) \\
& + (8l^4 - 7l^2b^2 + 8b^4)(M+3m) - 3d^4(M+5m) + 2(6l^2b^2(M+3m) \\
& + 4d^2(l^2+b^2)(M+3m) - 3d^4(M+4m))\cos\theta - (3d^4 - 3l^2b^2 - 2d^2(l^2+b^2)) \\
& \times (M+3m)\cos 2\theta)\sin 3\alpha + 32l^3b^4(M+3m)\cos\left(\tfrac{\theta}{2}\right)^4 \sin 5\alpha\Big)\Big),
\end{aligned}$$

$$M_{12} = \frac{l^3 l^2}{6d^5}\sin\theta\cos\alpha^3\left(-3d^2M + 2l^2M - 6d^2m + 6l^2m + 2ll(M+3m)\sin\alpha\right.$$
$$\left.-2(M+3m)\cos\theta\left(d^2 - 1^2 - ll\sin\alpha\right)\right),$$

$$M_{13} = \frac{l^2 b}{6d^6}\sin\theta\cos\alpha(lb^2(M+3m)\cos\alpha^2(-3d^2 + 2l^2 + 2b^2 + 6lb\sin\alpha$$
$$+ 2\cos\theta(-2d^2 + l^2 + b^2 + 3lb\sin\alpha)) + \tfrac{1}{2}(2d^4lM + 4d^2l^3M + d^2lb^2M$$
$$+ 2l^3b^2M + 2lb^4M + 12d^2l^3m + 3d^2lb^2m + 6l^3b^2m + 6lb^4m$$
$$+ lb^2(M+3m)\cos 2\alpha(2(l^2+b^2) - 3d^2 + 2(l^2 - 2d^2 + b^2)\cos\theta) + 2d^4bM\sin\alpha$$
$$+ 8d^2l^2bM\sin\alpha + l^2b^3M\sin\alpha + 24d^2l^2bm\sin\alpha + 3l^2b^3m\sin\alpha + l^2b^3M\sin 3\alpha$$
$$+ 3l^2b^3m\sin 3\alpha + b(M+3m)\cos\theta((-4d^4 + l^2b^2 + 4d^2(l^2+b^2))\sin\alpha$$
$$+ lb(2(2d^2 + l^2 + b^2) + lb\sin[3\alpha]))),$$

$$M_{14} = hlm\left(\cos\alpha\cos\phi_1 + \sin\alpha\cos\left(\beta - \theta_1\right)\sin\phi_1\right),$$
$$M_{15} = -hlm\sin\alpha\sin\left(\beta - \theta_1\right)\cos\phi_1,$$

$$M_{16} = \frac{hlm}{d^4}(\cos\phi^?2(\cos\alpha(d^2l^2 - (d^2+l^2)b^2 + 2b^4 + l^2b^2(\cos 2\alpha + 2\cos\alpha^2\cos\theta))$$
$$+ lb(d^2 - l^2 + b^2 + d^2\cos\theta\sin 2\alpha) + (\cos(\beta - \theta_2))(b^2\cos\theta(lb + (d^2+l^2)\sin\alpha))$$
$$+ l^2(lb + (d^2+b^2)\sin\alpha) + lb\cos 2\alpha(l^2 - d^2 + (b^2 - d^2)\cos\theta + lb(1+\cos\theta)\sin\alpha))$$
$$- db(lb\cos\alpha^2 + d^2\sin\alpha)\sin\theta\sin(\beta - \theta_2)\sin\phi_2),$$

$$M_{17} = \frac{hlm}{d^4}\cos\phi_2\left(-dlb^2\cos\alpha^2\cos\left(\beta - \theta_2\right)\sin\theta - d^3b\cos\left(\beta - \theta_2\right)\sin\alpha\sin\theta\right.$$
$$- \left(b^2\cos\theta\left(lb + \left(d^2+l^2\right)\sin\alpha\right) + l^2\left(lb + \left(d^2+b^2\right)\sin\alpha\right) + lb\cos\left(2\alpha\right)\right.$$
$$\left.\left.\times\ \left(-d^2 + l^2 + \left(-d^2+b^2\right)\cos\theta + lb(1+\cos\theta)\sin\alpha\right)\right)\sin\left(\beta - \theta_2\right)\right),$$

$$M_{21} = \frac{l^3b^2}{6d^5}\cos\alpha^3\left(-3d^2M + 2l^2M - 6d^2m + 6l^2m + 2lb(M+3m)\sin\alpha\right.$$
$$\left.-2(M+3m)\cos\theta\left(d^2 - b^2 - lb\sin\alpha\right)\right)\sin\theta,$$

$$M_{22} = \frac{l^2}{12d^4}\cos\alpha^2\left(4d^4(M+3m) + \left(4l^4 + 3l^2b^2 + 2b^4\right)(M+3m)\right.$$
$$+ 2d^2\left(2l^2M + b^2(M+3m)\right) + b\left(-l^2b(M+3m)\cos 2\alpha(3 + \cos 2\theta)\right.$$
$$+ 4l\left(d^2M + \left(2l^2 + b^2\right)(M+3m)\right)\sin\alpha + b(M+3m)$$
$$\times\cos 2\theta\left(-2d^2 + l^2 + 2b^2 + 4lb\sin\alpha\right) + 4\cos\theta(b + l\sin\alpha)$$
$$\left.\left.\times\left(d^2M + 2l^2(M+3m) + 2lb(M+3m)\sin\alpha\right)\right)\right),$$

$$M_{23} = \frac{1}{6d^3}l^2b\cos\alpha^2\left(2b(M+3m)(b + l\sin\alpha) + \cos\theta\left(d^2M + 2l^2(M+3m)\right.\right.$$
$$\left.\left.+2lb(M+3m)\sin\alpha\right)\right),$$

$$M_{24} = hlm\cos\alpha\sin\left(\beta - \theta_1\right)\sin\phi_1, \quad M_{25} = hlm\cos\alpha\cos[\beta - \theta_1]\cos[\phi_1],$$

$$M_{26} = \frac{1}{d^2}hlm\cos\alpha\left(\cos\theta_2\left(b\cos\theta(b + l\sin\alpha) + l(l + b\sin\alpha)\right)\sin\beta + db\cos\beta\sin\theta\right)$$
$$-(\cos\beta(b\cos\theta(b + l\sin\alpha) + l(l + b\sin\alpha)) - db\sin\beta\sin\theta)\sin\theta_2)\sin\phi_2,$$

$$M_{27} = \frac{1}{d^2} hlm \cos\alpha \cos\phi_2 \left(\cos\left(\beta - \theta_2\right) \left(b\cos\theta(b + l\sin\alpha) + l(l + b\sin\alpha)\right)\right.$$
$$\left. - db\sin\theta\sin\left(\beta - \theta_2\right)\right),$$

$$M_{31} = \frac{1}{6d^6} l^2 b\sin\theta\cos\alpha \left(l\left(d^4M + d^2\left(2l^2 - b^2\right)(M + 3m) + 2b^2\left(l^2 + b^2\right)(M + 3m)\right)\right.$$
$$+ b\left(2lb\left(l^2 + b^2\right)(M + 3m)\cos\theta + lb(M + 3m)\cos 2\alpha\left(-3d^2 + 2\left(l^2 + b^2\right)\right.\right.$$
$$\left.\left. + 2\left(l^2 - 2d^2 + b^2\right)\cos\theta\right) + \left(d^4M + 4d^2l^2(M + 3m) + 2l^2b^2(M + 3m)\right.\right.$$
$$\left.\left. - 2(d^4 - l^2b^2 - d^2(l^2 + b^2))\,(M + 3m)\cos\theta\right)\sin\alpha$$
$$\left. + 4l^2b^2(M + 3m)\cos\left(\tfrac{\theta}{2}\right)^2 \sin 3\alpha\right)\Big),$$

$$M_{32} = \frac{l^2 b}{6d^3}\cos\alpha^2\left((M + 3m)\left(2b(b + l\sin\alpha) + \cos\theta\sin\alpha(2l^2 + 2lb)\right) + d^2M\cos\theta\right),$$

$$M_{33} = \frac{l^2b^2(M + 3m)}{6d^4}\cos\alpha^2\left(d^2 + l^2 + b^2 + \left(d^2 - l^2 - b^2\right)\cos 2\theta + 4lb\sin\alpha\sin\theta^2\right),$$

$$M_{34} = 0, \quad M_{35} = 0,$$

$$M_{36} = \frac{hlbm}{d^2}\cos\alpha(l\cos\alpha\cos\phi_2\sin\theta + (\cos\left(\beta - \theta_2\right)(b + l\sin\alpha)\sin\theta$$
$$+ d\cos\theta\sin\left(\beta - \theta_2\right))\sin\phi_2),$$

$$M_{37} = \frac{hlbm}{d^2}\cos\alpha\cos\phi_2(d\cos\theta\cos\left(\beta - \theta_2\right) - (b + l\sin\alpha)\sin\theta\sin\left(\beta - \theta_2\right)),$$

$$M_{41} = hlm\left(\cos\alpha\cos\phi_1 + \sin\alpha\cos\left(\beta - \theta_1\right)\sin\phi_1\right),$$

$$M_{42} = hlm\cos\alpha\sin\left(\beta - \theta_1\right)\sin\phi_1, \quad M_{43} = 0, \quad M_{44} = h^2m,$$

$$M_{45} = 0, \quad M_{46} = 0, \quad M_{47} = 0,$$

$$M_{51} = -hlm\sin\alpha\sin\left(\beta - \theta_1\right)\cos\phi_1, \quad M_{52} = hlm\cos\alpha\cos\left(\beta - \theta_1\right)\cos\phi_1,$$

$$M_{53} = 0, \quad M_{54} = 0, \quad M_{55} = h^2m\cos\phi_1^2, \quad M_{56} = 0, \quad M_{57} = 0,$$

$$M_{61} = \frac{hlm}{d^4}\left(\cos\phi_2\left(\cos\alpha\left(d^2l^2 - \left(d^2 + l^2\right)b^2 + 2b^4 + l^2b^2\left(\cos 2\alpha + 2\cos\alpha^2\cos\theta\right)\right)\right.\right.$$
$$\left. + lb\left(d^2 - l^2 + b^2 + d^2\cos\theta\right)\sin 2\alpha\right) + \sin\phi_2\left(\cos\left(\beta - \theta_2\right)\left(b^2\cos\theta\,(lb\right.$$
$$\left. + (d^2 + l^2)\,\sin\alpha) + l^2\left(lb + \left(d^2 + b^2\right)\sin\alpha\right) + lb\cos 2\alpha\left(-d^2 + l^2 + (-d^2 + b^2)\right.\right.$$
$$\left.\left.\times\cos\theta + lb(1 + \cos\theta)\sin\alpha)\right) - db\left(lb\cos\alpha^2 + d^2\sin\alpha\right)\sin\theta\sin\left(\beta - \theta_2\right)\right)\Big),$$

$$M_{62} = \frac{hlm}{d^2}\sin\phi_2\cos\alpha(\cos\theta_2((b\cos\theta(b + l\sin\alpha) + l(l + b\sin\alpha))\sin\beta + db\cos\beta\sin\theta)$$
$$- \sin\theta_2(\cos\beta(b\cos\theta(b + l\sin\alpha) + l(l + b\sin\alpha)) - db\sin\beta\sin\theta)),$$

$$M_{63} = \frac{hlbm}{d^2}\cos\alpha\,(l\cos\alpha\cos\phi_2\sin\theta + \sin\phi_2\,(\cos(\beta-\theta_2)\,(b+l\sin\alpha)\sin\theta + d\cos\theta\sin(\beta-\theta_2)))\,,$$

$$M_{64}=0,\quad M_{65}=0,\quad M_{66}=h^2m,\quad M_{67}=0,$$

$$M_{71} = -\frac{hlm}{d^4}\cos\phi_2\left(d^2\sin\alpha\left(db\cos(\beta-\theta_2)\sin\theta+\sin(\beta-\theta_2)\left(l^2+b^2\cos\theta + lb(1+\cos\theta)\sin\alpha\right)\right) + lb\cos\alpha^2\left(db\cos(\beta-\theta_2)\sin\theta + \sin(\beta-\theta_2)\times\left(-d^2+2l^2-\left(d^2-2b^2\right)\cos\theta+2lb(1+\cos\theta)\sin\alpha\right)\right)\right),$$

$$M_{72} = \frac{hlm}{d^2}\cos\alpha\cos\phi_2\,(\cos(\beta-\theta_2)\,(b\cos\theta\,(b+l\sin\alpha)+l\,(l+b\sin\alpha)) - db\sin\theta\sin(\beta-\theta_2))\,,$$

$$M_{73} = \frac{hlbm}{d^2}\cos\alpha\cos\phi_2\,(d\cos\theta\cos(\beta-\theta_2)-\sin\theta\sin(\beta-\theta_2)\,(b+l\sin\alpha))\,,$$

$$M_{74}=0,\quad M_{75}=0,\quad M_{76}=0,\quad M_{77}=h^2m\cos\phi_2^2,$$

$$\begin{aligned}RR_1 = {}& \frac{1}{96d^{10}}l(2lb\cos\alpha\left(4l^3b^4(M+3m)\cos4\alpha\cos\left(\tfrac{\theta}{2}\right)^2\left(-53d^2+16\left(l^2+b^2\right)\right.\right.\\
&+\left(16\left(l^2+b^2\right)-59d^2\right)\cos\theta\big)+4lb^2\cos2\alpha\left(-3d^2\left(16l^4-17l^2b^2+16b^4\right)\right.\\
&\times(M+3m)+16\left(2l^6+l^4b^2+l^2b^4+2b^6\right)(M+3m)+6d^6(M+7m)\\
&-2d^4\left(13l^2(M+3m)+4b^2(M+6m)\right)+8\left(-8d^2l^2b^2(M+3m)+8l^2b^2(l^2+b^2)\right.\\
&\times(M+3m)+d^6(2M+9m)-3d^4(b^2(M+3m)+l^2(M+4m))\big)\cos\theta\\
&+\left(10d^6-6d^4l^2+\left(16l^4-8d^4-19d^2l^2\right)b^2+16l^2b^4\right)(M+3m)\cos2\theta)\\
&+l\left(-8d^8M-d^2b^2\left(64l^4-113l^2b^2+64b^4\right)(M+3m)+16b^2(8l^6+l^4b^2\right.\\
&+l^2b^4+8b^6)(M+3m)-24d^6\left(2l^2m+b^2(M+3m)\right)+8d^4(4l^4(M+3m)\\
&+5l^2b^2(M+3m)+2b^4(5M+9m)\big)-8\left(d^8M+4d^2l^2b^4(M+3m)\right.\\
&-24l^2b^4\left(l^2+b^2\right)(M+3m)+2d^6\left(l^2(M+3m)+b^2(2M+9m)\right)\\
&-4d^4b^2\left(b^2(M+3m)+l^2(5M+12m)\right)\big)\cos\theta+b^2\left(-24d^6-17d^2l^2b^2\right.\\
&+48l^2b^2\left(l^2+b^2\right)+8d^4\left(3l^2+2b^2\right)\big)(M+3m)\cos2\theta)+4b\left(-6d^8(M+m)\right.\\
&+8l^2b^2\left(4l^4-5l^2b^2+4b^4\right)(M+3m)+2d^2\left(8l^6+7l^4b^2+7l^2b^4+8b^6\right)\\
&\times(M+3m)+d^6\left(2b^2(5M+3m)-4l^2(M+6m)\right)+d^4b^2\left(-16b^2(M+3m)\right.\\
&+l^2(47M+129m)\big)+4\left(-d^8M+d^6l^2(M-6m)+8l^4b^4(M+3m)\right.\\
&+10d^2l^2b^2\left(l^2+b^2\right)(M+3m)+d^4l^2\left(4l^2(M+3m)+b^2(5M+12m)\right)\big)\cos\theta\\
&+\left(2d^8-2d^6b^2+5d^4l^2b^2+8l^4b^4+10d^2l^2b^2\left(l^2+b^2\right)\right)(M+3m)\cos2\theta\big)\sin\alpha\\
&+4l^2b^3\left(30d^2\left(l^2+b^2\right)(M+3m)+4\left(8l^4-7l^2b^2+8b^4\right)(M+3m)\right.\\
&-d^4(41M+135m)+4\left(12l^2b^2(M+3m)+10d^2\left(l^2+b^2\right)(M+3m)\right.\\
&-3d^4(5M+16m)\big)\cos\theta-\left(19d^4-12l^2b^2-10d^2\left(l^2+b^2\right)\right)(M+3m)\cos2\theta)\\
&\times\sin3\alpha+128l^4b^5(M+3m)\cos\left(\tfrac{\theta}{2}\right)^4\sin5\alpha\Big)\alpha'^2+8d^2lb\left(\left(2b\left(d^6M-2d^2l^2b^2\right.\right.\right.\end{aligned}$$

$$\times(M+3m)+\ 6l^2b^2\left(l^2+b^2\right)(M+3m)+\ \ 2d^4l^2(4M+9m)\big)+2b\left(-d^6M$$
$$-6d^4l^2m-8d^2l^2b^2(M+3m)+8l^2b^2\left(l^2+b^2\right)(M+3m)\big)\cos 2\alpha$$
$$+l\left(lb^3(M+3m)\cos 4\alpha\left(4\left(-3d^2+l^2+b^2\right)+\left(-13d^2+4\left(l^2+b^2\right)\right)\cos\theta\right)\right.$$
$$+4\left(d^6M+5l^2b^4(M+3m)+4d^2b^2\left(l^2+b^2\right)(M+3m)+d^4\left(2l^2(M+3m)\right.\right.$$
$$\left.-b^2(M+6m)\right)+b^2\left(\left(6l^2b^2(M+3m)+4d^2\left(l^2+b^2\right)(M+3m)\right.\right.$$
$$\left.\left.-3d^4(M+4m)\right)\cos 2\alpha+(M+3m)\left(-2d^4+5l^2b^2+4d^2\left(l^2+b^2\right)\right.\right.$$
$$\left.\left.+\left(-6d^4+6l^2b^2+4d^2\left(l^2+b^2\right)\right)\cos 2\alpha\right)\cos\theta\right)\sin\alpha\big)\big)\sin\theta$$
$$+2l^3b^4(M+3m)\csc\left(\tfrac{\theta}{2}\right)^2\sin 5\alpha\sin\theta^3+\tfrac{1}{2}b(M+3m)\left(-4d^6-7d^2l^2b^2\right.$$
$$+12l^2b^2\left(l^2+b^2\right)+4d^4\left(2l^2+b^2\right)+\ 4\left(d^6-\left(d^4+5d^2l^2-4l^4\right)b^2\right.$$
$$\left.+4l^2b^4\right)\cos 2\alpha\big)\sin 2\theta\big)\,\alpha'\theta'-4d^4\left(l\cos\alpha\left(-8l^3b^3(M+3m)\cos 4\alpha\cos\left(\tfrac{\theta}{2}\right)^4\right.\right.$$
$$+lb\big(2d^4M+\left(8l^4+3l^2b^2+4b^4\right)(M+3m)+4d^2(b^2(M+3m)+\ l^2(2M+3m))$$
$$+2\left(d^4M+10l^2b^2(M+3m)+2d^2\left(l^2(M+3m)+b^2(2M+3m)\right)\right)\cos\theta$$
$$+b^2\big(l^2+4b^2\big)(M+3m)\cos 2\theta\big)+2\left(4d^6(M+3m)+2l^2b^2\left(2l^2+b^2\right)(M+3m)\right.$$
$$+2d^4\left(2l^2M+b^2(M+3m)\right)+d^2\left(4l^4(M+3m)+2b^4(M+3m)\right.$$
$$\left.+\ l^2b^2(4M+9m)\right)+b^2\left(\left(4d^4M+4l^2\left(l^2+b^2\right)(M+3m)\right.\right.$$
$$\left.\left.+d^2l^2(13M+36m)\right)\cos\theta+\ 2\left(-d^4+\left(d^2+2l^2\right)b^2\right)(M+3m)\cos 2\theta\big)\big)\sin\alpha$$
$$+2lb\cos 2\alpha\left(-3d^4M+2\left(2l^4+b^4\right)(M+3m)-2d^2\left(b^2(M+3m)\right.\right.$$
$$\left.+l^2(2M+9m)\right)-\left(3d^4M-8l^2b^2(M+3m)+2d^2\left(3l^2(M+3m)\right.\right.$$
$$\left.\left.+b^2(2M+9m)\right)\right)\cos\theta+\ 2b(M+3m)\cos 2\theta\left(b^3-2d^2b-l\left(d^2-2b^2\right)\sin\alpha\right)\big)$$
$$+2l^2b^2\left(2\left(2l^2+b^2\right)(M+3m)-\ d^2(2M+9m)+\left(4\left(l^2+b^2\right)(M+3m)\right.\right.$$
$$\left.\left.-\ \ 3d^2(M+4m)\right)\cos\theta\right)\sin 3\alpha\big)\,\beta'^2+2dlb\cos\alpha\left(4lb(M+3m)\cos\alpha^2\cos 2\theta\right.$$
$$\times\left(b^2-d^2+\ lb\sin\alpha\right)+2b(M+3m)\left(l\left(d^2+3b^2\right)+\left(4d^2+3l^2\right)b\sin\alpha\right)$$
$$+2lb(M+3m)\cos 2\alpha\left(4\left(l^2-d^2\right)\cos\theta+3\left(b^2-d^2+lb\sin\alpha\right)\right)$$
$$+4\cos\theta\left(\left(d^4M+2d^2l^2(M+3m)+l^2b^2(M+3m)\right)\sin\alpha+l^2b(M+3m)\right.$$
$$\left.\times(2l+b\sin 3\alpha)\big)\big)\,\beta'\theta'+4lb\cos\alpha\left(2lb^2(M+3m)\cos 2\alpha\cos\left(\tfrac{\theta}{2}\right)^2\right.$$
$$\times\left(d^2+\ 2\left(-2d^2+l^2+b^2\right)\cos\theta\right)+l\left(\left(d^4M+d^2\left(2l^2-b^2\right)(M+3m)\right.\right.$$
$$\left.\left.+2b^2\big(l^2+b^2\big)(M+3m)\right)\cos\theta+b^2(M+3m)\big(d^2+l^2+b^2+\left(l^2+b^2\right)\cos 2\theta\big)\right)$$
$$+b\left(\left(d^4M+4d^2l^2(M+3m)+2l^2b^2(M+3m)\right)\cos\theta+(M+3m)((d^2+l^2)\right.$$
$$\left.\times\left(d^2+b^2\right)+\left(l^2b^2-d^4+d^2\left(l^2+b^2\right)\right)\cos 2\theta\right)\big)\sin\alpha+4l^2b^3(M+3m)$$
$$\left.\times\cos\left(\tfrac{\theta}{2}\right)^2\cos\theta\sin 3\alpha\right)\theta'^2+12d^2\left(\tfrac{1}{2}g(M+2m)\left(2\cos\beta\left(l^3b+d^4\sin\alpha\right.\right.\right.$$
$$\left.\left.\left.+l^2\left(d^2+b^2\right)\sin\alpha+lb\cos 2\alpha\left(l^2-d^2+\left(b^2-d^2\right)\cos\theta+lb\sin\alpha\right)\right.\right.\right.$$
$$\left.\left.+\ b^2\cos\theta\left(lb+\left(d^2+2l^2\cos\alpha^2\right)\sin\alpha\right)\right)-\ 2db\left(lb\cos\alpha^2+d^2\sin\alpha\right)\sin\beta\sin\theta\big)$$
$$+2d^4hm\cos\left(\beta-\theta_1\right)\cos\phi_1\sin\alpha\theta_1'^2+hm\cos\phi_2(2\cos\left(\beta-\theta_2\right)$$
$$\times\left(b^2\cos\theta\left(lb+\ \left(d^2+l^2\right)\sin\alpha\right)+l^2\left(lb+\left(d^2+b^2\right)\sin\alpha\right)+\ lb\cos 2\alpha\left(l^2-d^2\right.\right.$$
$$\left.\left.+(b^2-d^2)\cos\theta+\ lb(1+\cos\theta)\sin\alpha\right)\right)-2db\left(lb\cos\alpha^2+d^2\sin\alpha\right)$$
$$\left.\times\sin\theta\sin\left(\beta-\theta_2\right)\right)\theta_2'^2+4d^4hm\theta_1'\phi_1'\sin\alpha\sin\left(\beta-\theta_1\right)\sin\phi_1$$

$$
\begin{aligned}
&+4hm\left(dlb^2\cos\alpha^2\cos\left(\beta-\theta_2\right)\sin\theta+\ d^3b\cos\left(\beta-\theta_2\right)\sin\alpha\sin\theta\right.\\
&+\left(b^2\cos\theta\left(lb+\left(d^2+l^2\right)\sin\alpha\right)+l^2\left(lb+\left(d^2+b^2\right)\sin\alpha\right)+lb\cos 2\alpha(-d^2+l^2\right.\\
&\left.+(b^2-d^2)\cos\theta+lb(1+\cos\theta)\sin\alpha)\right)\sin\left(\beta-\theta_2\right)\Big)\sin\phi_2\theta_2'\phi_2'+2hm\\
&\times\left(d^4\left(\cos\left(\beta-\theta_1\right)\cos\phi_1\ \ \sin\alpha-\cos\alpha\sin\phi_1\right)\phi_1'^2+\left(\cos(\beta-\theta_2)\cos\phi_2\right.\right.\\
&\times\left(b^2\cos\theta(lb+(d^2+l^2)\sin\alpha)+\ l^2\left(lb+\left(d^2+b^2\right)\sin\alpha\right)+lb\cos 2\alpha(l^2-d^2\right.\\
&\left.+(b^2-d^2)\cos\theta+lb(1+\cos\theta)\sin\alpha)\right)-db\cos\phi_2\left(lb\cos\alpha^2+d^2\sin\alpha\right)\\
&\times\sin\theta\sin\left(\beta-\theta_2\right)-\cos\alpha\left(d^2l^2-\left(d^2+l^2\right)b^2+2b^4+lb\left(lb(\cos 2\alpha\right.\right.\\
&\left.\left.\left.\left.+2\cos\alpha^2\cos\theta)+\ 2\left(d^2-l^2+b^2+d^2\cos\theta\right)\sin\alpha\right)\right)\sin\phi_2\right)\phi_2'^2\Big)\Big)\Big),
\end{aligned}
$$

$$
\begin{aligned}
RR_2=&\frac{1}{48d^7}l\cos\alpha(2l^2b^2\cos\alpha(2(lb(10l^2(M+3m)-d^2(5M+6m))+lb(10l^2(M+3m)\\
&-d^2(17M+42m))\cos 2\alpha+(-18d^4(M+2m)+12d^2l^2(M+3m)\\
&+5l^2b^2(M+3m))\sin\alpha+5l^2b^2(M+3m)\sin 3\alpha)\sin\theta+(M+3m)\\
&\times(2(b^2(6d^2+5l^2)-6d^4)-2lb(d^2-5b^2))\sin\alpha+2lb\cos 2\alpha(5b^2-7d^2\\
&+5lb\sin\alpha))\sin 2\theta)\alpha'^2+4dl\alpha'((-8l^3b^3(M+3m)\cos 4\alpha\cos(\tfrac{\theta}{2})^4+lb(2d^4M\\
&+(8l^4+3l^2b^2+4b^4)(M+3m)+4d^2(b^2(M+3m)+l^2(2M+3m))\\
&+2(d^4M+10l^2b^2(M+3m)+2d^2(l^2(M+3m)+b^2(2M+3m)))\cos\theta\\
&+b^2(l^2+4b^2)(M+3m)\cos 2\theta)+2(4d^6(M+3m)+2l^2b^2(2l^2+b^2)(M+3m)\\
&+2d^4(2l^2M+b^2(M+3m))+d^2(4l^4(M+3m)+2b^4(M+3m)\\
&+l^2b^2(4M+9m))+b^2((4d^4M+4l^2(l^2+b^2)(M+3m)\\
&+d^2l^2(13M+36m))\cos\theta+2(-d^4+(d^2+2l^2)b^2)(M+3m)\cos 2\theta))\sin\alpha\\
&+2lb\cos 2\alpha(2(2l^4+b^4)(M+3m)-3d^4M-2d^2(b^2(M+3m)+l^2(2M+9m))\\
&-(3d^4M-8l^2b^2(M+3m)+2d^2(3l^2(M+3m)+b^2(2M+9m)))\cos\theta\\
&+2b(M+3m)\cos 2\theta(b^3-2d^2b-l(d^2-2b^2)\sin\alpha))+2l^2b^2(2(2l^2+b^2)(M+3m)\\
&-d^2(2M+9m)+(4(l^2+b^2)(M+3m)-3d^2(M+4m))\cos\theta)\sin 3\alpha)\beta'\\
&+db(-4lb(M+3m)\cos\alpha^2\cos 2\theta(b^2-d^2+lb\sin\alpha)+4\cos\theta(lb\cos\alpha^2\\
&+d^2\sin\alpha)(d^2M+2l^2(M+3m)+2lb(M+3m)\sin\alpha)+b(M+3m)(2l(d^2+3b^2)\\
&+2(4d^2+3l^2)b\sin\alpha+6l\cos 2\alpha(b^2-d^2+lb\sin\alpha)))\theta')\\
&+d^3(8lb\cos\alpha(2(b+l\sin\alpha)(d^2M+2l^2(M+3m)+2lb(M+3m)\sin\alpha)\sin\theta\\
&+b(M+3m)(l^2-2d^2+2b^2-l^2\cos 2\alpha+4lb\sin\alpha)\sin 2\theta)\beta'\theta'\\
&+4d(2lb\cos\alpha(d^2M+2l^2(M+3m)+2lb\theta'^2(M+3m)\sin\alpha)\sin\theta\\
&+6d(g(M+2m)(-(d^2+l^2+lb\sin\alpha+b\cos\theta(b+l\sin\alpha))\sin\beta-db\cos\beta\sin\theta)\\
&+hm(-2(d^2\cos\phi_1\sin(\beta-\theta_1)\theta_1'^2+\cos\phi_2(db\cos(\beta-\theta_2)\sin\theta+(l^2+b^2\cos\theta\\
&+lb(1+\cos\theta)\sin\alpha)\sin(\beta-\theta_2))\theta_2'^2-2d^2\cos(\beta-\theta_1)\sin\phi_1\theta_1'\phi_1'\\
&+d^2\cos\phi_1\sin(\beta-\theta_1)\phi_1'^2)+4(\sin\beta(-db\cos\theta_2\sin\theta+(l^2+b^2\cos\theta\\
&+lb(1+\cos\theta)\sin\alpha)\sin\theta_2)+\cos\beta(\cos\theta_2(l^2+b^2\cos\theta+lb(1+\cos\theta)\sin\alpha)\\
&+db\sin\theta\sin\theta_2))\theta_2'\phi_2'\sin\phi_2-2\cos\phi_2(db\cos(\beta-\theta_2)\sin\theta+(b\cos\theta(b+l\sin\alpha)\\
&+l(l+b\sin\alpha))\sin(\beta-\theta_2))\phi_2'^2)))),
\end{aligned}
$$

$$
\begin{aligned}
RR_3=&-\frac{1}{12d^8}lb\cos\alpha(6d^6g(M+2m)(d\cos\theta\sin\beta+\cos\beta(b+l\sin\alpha)\sin\theta)\\
&+lb\cos\alpha(-2(8d^2l^4(M+3m)-d^6M-6d^4l^2(M+3m)
\end{aligned}
$$

$$
\begin{aligned}
&+8l^2b^2(l^2+b^2)(M+3m)+2lb(M+3m)((2d^2-5d^4+8l^2b^2(5l^2+b^2))\sin\alpha\\
&+4lb\cos 2\alpha(l^2+b^2-2d^2+2lb\sin\alpha)))\sin\theta-(M+3m)(2d^6+5d^2l^2b^2\\
&+8l^2b^2(l^2+b^2)-2d^4(2l^2+b^2)+lb(4(-4d^4+4l^2b^2+3d^2(l^2+b^2))\sin\alpha\\
&+lb\cos 2\alpha(-19d^2+8(l^2+b^2)+16lb\sin\alpha)))\sin 2\theta)\alpha'^2\\
&+d^2l\alpha'(4d\cos\theta(2(d-l)l(d+l)b(M+3m)\cos 2\alpha-(d^4M+2d^2l^2(M+3m)\\
&+l^2b^2(M+3m))\sin\alpha-l^2b(M+3m)(2l+b\sin 3\alpha))\beta'+b(M+3m)\\
&\times\cos 2\theta(-4dl\cos\alpha^2(b^2-d^2+lb\sin\alpha)\beta'+4(lb(l^2-2d^2+b^2)\cos 2\alpha\\
&+(l^2b^2-d^4+d^2(l^2+b^2))\sin\alpha+lb(l^2+b^2+lb\sin 3\alpha))\theta')\\
&+b(M+3m)(-d(2l(d^2+3b^2)+2(4d^2+3l^2)b\sin\alpha+6l\cos 2\alpha(b^2-d^2\\
&+lb(l^2-d^2+b^2)\cos 2\alpha-(d^2+l^2)(d^2+b^2)\sin\alpha-lb(d^2+l^2+b^2\\
&+lb\sin 3\alpha))\theta'))+d^4(l\cos\alpha(2(b+l\sin\alpha)(d^2M+2l^2(M+3m)\\
&+2lb(M+3m)\sin\alpha)\sin\theta+b(M+3m)(l^2-2d^2+2b^2-l^2\cos 2\alpha\\
&+4lb\sin\alpha)\sin 2\theta)\beta'^2+2lb(M+3m)\theta'^2\cos\alpha(l^2-d^2+b^2+2lb\sin\alpha)\sin 2\theta\\
&+12d^2hm\phi_2'\sin\phi_2(2(-d\cos\theta\cos(\beta-\theta_2)+(b+l\sin\alpha)\sin\theta\sin(\beta-\theta_2))\theta_2'\\
&-l\cos\alpha\sin\theta\phi_2')+3d^2hm\cos\phi_2(4\cos(\beta-\theta_2)(b+l\sin\alpha)\sin\theta\\
&+4d\cos\theta\sin(\beta-\theta_2))(\theta_2'^2+\phi_2'^2))),
\end{aligned}
$$

$$
\begin{aligned}
RR_4=&-hm(l(-\cos\phi_1\sin\alpha+\cos\alpha\cos(\beta-\theta_1)\sin\phi_1)\alpha'^2\\
&-2l\sin\alpha\sin(\beta-\theta_1)\sin\phi_1\alpha'\beta'+\sin\phi_1(g\cos\theta_1+l\cos\alpha\cos(\beta-\theta_1)\beta'^2\\
&+h\cos\phi_1\theta_1'^2)),
\end{aligned}
$$

$$
\begin{aligned}
RR_5=&\,hm\cos\phi_1\left(-g\sin\theta_1+l\alpha'^2\cos\alpha\sin(\beta-\theta_1)+2l\alpha'\beta'\cos(\beta-\theta_1)\sin\alpha\right.\\
&\left.+l\cos\alpha\sin(\beta-\theta_1)\beta'^2+2h\theta_1'\phi_1'\sin\phi_1\right),
\end{aligned}
$$

$$
\begin{aligned}
RR_6=&-\frac{1}{d^6}hm(-l(8l^3b^3\cos\alpha^4\cos\theta\cos\phi_2+d^2\cos\phi_2\sin\alpha(2b^4+d^2(l-b)(l+b)\\
&+2lb\sin\alpha(d^2-l^2+b^2+d^2\cos\theta-lb\sin\alpha))-2lb\cos\alpha^2\cos\phi_2(d^4-2d^2l^2\\
&+2b^2(d^2+l^2)-4b^4+d^4\cos\theta+lb(-2lb\cos 2\alpha-(4(d^2-l^2+b^2)\\
&+5d^2\cos\theta)\sin\alpha))+\tfrac{1}{2}\cos\alpha(2\cos(\beta-\theta_2)(l^2(-d^4+(d^2+4l^2)b^2)\\
&+b(b(-d^4+d^2l^2+4l^2b^2)\cos\theta+l^2b\cos 2\alpha(-5d^2+4l^2+(-5d^2+4b^2)\cos\theta)\\
&+2l(-2d^4+3d^2l^2+l^2b^2+(-2d^4+(3d^2+l^2)b^2)\cos\theta)\sin\alpha\\
&+4l^3b^2\cos(\tfrac{\theta}{2})^2\sin 3\alpha))+db(2d^4-3l^2b^2-3lb(lb\cos 2\alpha+2d^2\sin\alpha))\\
&\times\sin\theta\sin(\beta-\theta_2))\sin\phi_2)\alpha'^2-2d^2l\alpha'((d^2\sin\alpha(db\cos(\beta-\theta_2)\sin\theta\\
&+(l^2+b^2\cos\theta+lb(1+\cos\theta)\sin\alpha)\sin(\beta-\theta_2))+lb\cos\alpha^2(db\cos(\beta-\theta_2)\sin\theta\\
&+(2l^2-d^2-(d^2-2b^2)\cos\theta+2lb(1+\cos\theta)\sin\alpha)\sin(\beta-\theta_2)))\beta'\sin\phi_2\\
&+b(l\cos\phi_2(2lb\cos\alpha^3+d^2\sin 2\alpha)\sin\theta+(\cos(\beta-\theta_2)(d^2\sin\alpha(b+l\sin\alpha)\\
&+l\cos\alpha^2(2b^2-d^2+2lb\sin\alpha))\sin\theta+d\cos\theta(lb\cos\alpha^2+d^2\sin\alpha)\\
&\times\sin(\beta-\theta_2))\sin\phi_2)\theta')+d^4(l\cos\alpha(\sin\beta(-db\cos\theta_2\sin\theta+(l^2+b^2\cos\theta\\
&+lb(1+\cos\theta)\sin\alpha)\sin\theta_2)+\cos\beta(\cos\theta_2(l^2+b^2\cos\theta+lb(1+\cos\theta)\sin\alpha)\\
&+db\sin\theta\sin\theta_2))\beta'^2\sin\phi_2+2lb\cos\alpha(d\cos\theta\cos(\beta-\theta_2)-(b+l\sin\alpha)\\
&\times\sin\theta\sin(\beta-\theta_2))\beta'\theta'\sin\phi_2+lb\cos\alpha(l\cos\alpha\cos\theta\cos\phi_2\\
&+(\cos\theta\cos(\beta-\theta_2)(b+l\sin\alpha)-d\sin\theta\sin(\beta-\theta_2))\theta'^2\sin\phi_2)\\
&+d^2\sin\phi_2(g\cos\theta_2+h\cos\phi_2\theta_2'^2))),
\end{aligned}
$$

$$
\begin{aligned}
RR_7 = -\frac{1}{d^6} hm\cos\phi_2 (l(d^2 lb(-2d^2+3l^2+(3b^2-2d^2)\cos\theta)\sin 2\alpha\sin(\beta-\theta_2) \\
+ l^2 b^2\cos\alpha^3(3db\cos(\beta-\theta_2)\sin\theta - 4(d^2-2l^2+(d^2-2b^2)\cos\theta \\
- 2lb(1+\cos\theta)\sin\alpha)\sin(\beta-\theta_2)) + d^2\cos\alpha(-db\cos(\beta-\theta_2) \\
\times(d^2-3lb\sin\alpha)\sin\theta - (l^2(d^2-3b^2)+b^2(d^2\cos\theta+3l^2(\cos 2\alpha \\
-2\cos\theta\sin\alpha^2)))\sin(\beta-\theta_2)))\alpha'^2 + d^2 l\alpha'(-l\cos(\beta-\theta_2)(2b\cos 2\alpha(l^2-d^2 \\
+ lb\sin\alpha) + 2l(lb+(d^2+b^2)\sin\alpha))\beta' + b\cos\theta\cos(\beta-\theta_2)(-(2b(lb \\
+ (d^2+l^2)\sin\alpha) + 2l\cos 2\alpha(b^2-d^2+lb\sin\alpha))\beta' - 2d(lb\cos\alpha^2+d^2\sin\alpha)\theta') \\
+ b\sin\theta\sin(\beta-\theta_2)(2(dlb\cos\alpha^2+d^3\sin\alpha)\beta' + (2b(lb+(d^2+l^2)\sin\alpha) \\
+ 2l\cos 2\alpha(-d^2+b^2+lb\sin\alpha))\theta')) + d^4(d^2 g\sin\theta_2 + l\cos\alpha(-l(l+b\sin\alpha) \\
\times\sin(\beta-\theta_2)\beta'^2 - b\cos(\beta-\theta_2)\sin\theta(d\beta'^2 + 2(b+l\sin\alpha)\beta'\theta' + d\theta'^2) \\
-b\cos\theta\sin(\beta-\theta_2)((b+l\sin\alpha)\beta'^2 + 2d\beta'\theta' + (b+l\sin\alpha)\theta'^2)) \\
-2d^2 h\sin\phi_2\theta_2'\phi_2')).
\end{aligned}
$$

References

1. R. Dilao, Chaos **19**, 023118 (2009)
2. M. Bennett, M.F. Schatz, H. Rockwood, K. Wiesenfeld, Proc. R. Soc. Lond. A **458**, 563 (2002)
3. Sz. Boda, Z. Neda, B. Tyukodi, A. Tunyagi, Eur. Phys. J. B **86**, 263 (2013)
4. J. Pantaleone, Am. J. Phys. **70**, 992 (2002)
5. I.I. Blekhman, *ASME Press* (New York, 1988)
6. A. Pogromsky, V.N. Belykh, H. Nijmeijer, Proceedings of the 42nd IEEE Conference on Design and Control, 4381 (2003)
7. M. Senator, J. Sound Vib. **291**, 566 (2006)
8. K. Czolczynski, P. Perlikowski, A. Stefanski, T. Kapitaniak, Physica A **388**, 5013 (2009)
9. K. Czolczynski, P. Perlikowski, A. Stefanski, T. Kapitaniak, Commun. Nonlinear Sci. Numer. Simul. **18**, 386 (2013)
10. K. Czolczynski, P. Perlikowski, A. Stefanski, T. Kapitaniak, Chaos: An Interdisciplinary J. Nonlinear Sci. **21**, 023129 (2011)
11. K. Czolczynski, P. Perlikowski, A. Stefanski, T. Kapitaniak, Prog. Theor. Phys. **125**, 1 (2011)
12. M. Kapitaniak, P. Perlikowski, T. Kapitaniak, Commun. Nonlinear Sci. Numer. Simul. **18**, 2088 (2013)
13. M. Kapitaniak, P. Brzeski, K. Czolczynski, P. Perlikowski, A. Stefanski, T. Kapitaniak, Progr. Theor. Phys. **128**, 1141 (2012)
14. M. Kapitaniak, K. Czolczynski, P. Perlikowski, A. Stefanski, T. Kapitaniak, Phys. Reports **517**, 1 (2012)
15. P. Perlikowski, M. Kapitaniak, K. Czolczynski, A. Stefanski, T. Kapitaniak, Int. J. Bifur. Chaos **22**, 1250288 (2012)
16. K. Czolczynski, P. Perlikowski, A. Stefanski, T. Kapitaniak, Int. J. Bifur. Chaos **22**, 1250128 (2012)
17. K. Czolczynski, P. Perlikowski, A. Stefanski, T. Kapitaniak, Commun. Nonlinear Sci. Numer. Simul. **17**, 3658 (2011)
18. M.G. Olsson, Am. J. Phys. **46**, 1118 (1978)
19. M.G. Olsson, Am. J. Phys. **49**, 531 (1981)
20. S. Leyendecker, P. Betsch, P. Steinmann, Comput. Mech., 174 (2004)
21. TJ. Priest, J. Poth, The Physics Teacher (1982)
22. H.C. Mayer, R. Krechetnikov, Phys. Rev. E, 046117 (2012)
23. J. Strzalko, B. Mianowski, Wydawnictwo Politechniki Lodzkiej, 162 (1985)

PAPER B

Eur. Phys. J. Special Topics **223**, 707–720 (2014)

DOI: 10.1140/epjst/e2014-02136-8

THE EUROPEAN PHYSICAL JOURNAL SPECIAL TOPICS

Regular Article

The dynamics of co- and counter rotating coupled spherical pendula

B. Witkowski[1], P. Perlikowski[1,a], A. Prasad[2], and T. Kapitaniak[1]

[1] Division of Dynamics, Technical University of Lodz, 90-924 Lodz, Stefanowskiego 1/15, Poland
[2] Department of Physics and Astrophysics, University of Delhi, Delhi 110007, India

Received 3 March 2014 / Received in final form 18 March 2014
Published online 28 April 2014

Abstract. The dynamics of co- and counter-rotating coupled spherical pendula (two lower pendula are mounted at the end of the upper pendulum) is considered. Linear mode analysis shows the existence of three rotating modes. The linear modes allow us to understand the nonlinear normal modes, which are visualized in frequency-energy plots. With the increase of energy in one mode we observe a symmetry breaking pitchfork bifurcation. In the second part of the paper we consider energy transfer between pendula having different energies. The results for co-rotating (all pendula rotate in the same direction) and counter-rotating motion (one of lower pendula rotates in the opposite direction) are presented. In general, the energy fluctuations in counter-rotating pendula are found to be higher than in the co-rotating case.

1 Introduction

Coupled oscillators can exhibit complex phenomena such as: energy flows, synchronization, beating, internal resonances, amplitude death, chaotic and quasiperiodic transients etc. [1–8]. There are numerous studies on the dynamics of the pendulum, single or coupled, but mostly devoted to in-plane oscillations [9–11]. In our studies we investigate the behavior of the coupled spherical pendula. The first description of spherical pendulum dynamics has been presented by Olssen [12,13], who derived the equations of motion and solved them analytically using Lindstedt-Poincare method. The obtained solution shows periodic rotation of pendulum for small but finite displacements. The spherical pendulum is often taken as a model in quantum mechanics, for example in Refs. [14,15] where the authors consider a Hamiltonian system showing its asymptotic properties. In Ref. [16] the spherical pendulum is taken as an example to show different ways of solving Hamiltonian system with holonomic constrains. The authors show that the Penalty Method can compete with the Lagrange Multiplier Method and the choice of the method depends on the complexity of the problem and its expected accuracy. The dynamics of spherical pendulum for increasing value of energy is presented in Ref. [17] where the authors consider several energy levels and

[a] e-mail: przemyslaw.perlikowski@p.lodz.pl

present, using analytical and numerical tools, general scenarios of bifurcations. The global nonlinear stable manifolds of the spherical pendulum hyperbolic equilibrium with closed loop attitude control are analyzed by Lee *et al.* [18]. Their investigations have led us to understand the global stabilization properties of closed loop control systems on nonlinear spaces. The consequence of symmetry breaking including PT-transition is shown in Ref. [19]. The spherical pendulum is also used to model an arm carrying a cup of coffee [20].

The dynamics of double pendulum has been considered in Ref. [21] where the author used the model consisting of two rigid rods with elastic joints with the force acting parallel to lower pendulum. The detailed stability analysis based on the center manifold theorem has been considered for hanging down position. Here, the period motion under the varying external force and damping coefficient have been studied. In another work [22] the general theory of Lagrangian reduction is applied to the equations of motion to simplify the problem where the main form of vibrations and its bifurcations are observed. The symmetric properties of spherical pendulum motion are investigated in details by Chossat and Bou-Rabee [23]. When the symmetry is present in the system one can observe a symmetric quasiperiodic and chaotic motions separated by heteroclinic connections. The reduction of cyclic symmetries or symmetry breakdown leads to an immediate change of motion. The analytical investigation including the analysis of double spherical pendulum topology was conducted by Hu *et al.* [24]. Their work has led us to understand the geometric as well as the dynamical properties of the systems.

In this paper we analyze the rotational motion of three coupled spherical pendula. Using the linear approximation theory we obtain three independent linear modes of the pendulum's rotation. In each mode the pendula rotate in clock-wise direction with different phase shifts and different amplitudes. Based on these linear mode solutions we estimate nonlinear normal modes [25–27] using path-following algorithm. With the increase of total energy of the system the frequencies of the modes also increase. However, for higher energy level, the symmetry breaking pitchfork bifurcation occurs in first mode. For periodic solutions there is no transfer of energy between the pendula. The energy flows among the pendula for the co-rotating and counter-rotating rotations are discussed. In general, the energy fluctuation in counter-rotating pendula are found to be higher than in co-rotating case.

The paper is organized as follows. The considered model of the coupled spherical pendulum is introduced in Sect. 2. Section 3 contains the derivation of the eigenfrequencies and eigenvectors of the linearized systems. We use path-following algorithm to obtain linear solution for increasing energy of the system. The discussion on nonlinear normal modes is presented in Sect. 4. The energy flows between the pendula are discussed in Sect. 5. The conclusions of the results are summarized in Sect. 6.

2 Model of two coupled spherical pendula

We consider the system composed of an upper and two lower spherical pendula as shown schematically in Fig. 1. The upper pendulum with mass M is suspended on weightless and inextensible strings of length L. At the end of the upper pendulum two identical pendula are suspended, each of length H and mass m. The motion of upper pendulum is described by two angles φ and θ as shown in Fig. 1, where φ is the angle between the string L and the plane YZ, while angle θ represents the angular position of the pendulum around axis X. Motions of the first and the second lower pendulum are described in the same manner by variables φ_1 & θ_1 and φ_2 & θ_2 respectively. This system is Hamiltonian as there is neither external force nor dissipation of energy due to any type of frictional force.

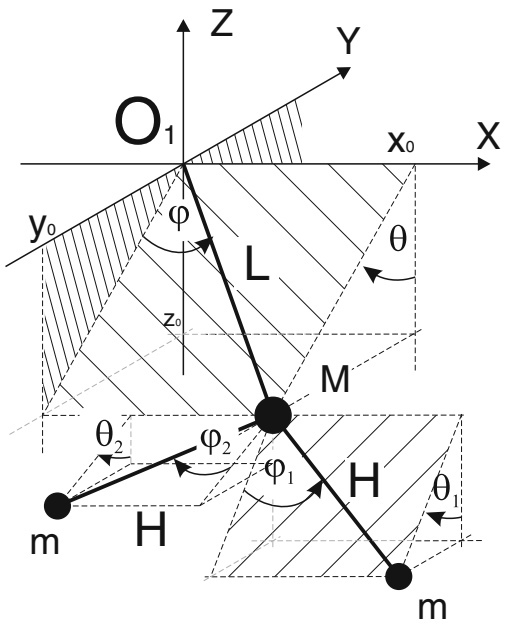

Fig. 1. Schematic figure for the coupled pendulum.

In Cartesian coordinates the upper pendulum can be written using transformation: $x_0 = L\sin\varphi$, $y_0 = L\sin\theta\cos\varphi$ and $z_0 = -L\cos\theta\cos\varphi$. Similarly, for each pendulum the coordinates can be written as follows: $x_i = H\sin\varphi_i + x_0$, $y_i = H\sin\theta_i\cos\varphi_i + y_0$ and $z_i = -H\cos\theta_i\cos\varphi_i + z_0$, where $i = 1, 2$. The kinetic energy is composed of the energy of the upper pendulum and the energy of two lower pendula. For upper pendulum this energy is given by:

$$T_M = \frac{1}{2}M(\dot{x}_0^2 + \dot{y}_0^2 + \dot{z}_0^2) = \frac{1}{2}L^2M\left(\cos^2\varphi\dot{\theta}^2 + \dot{\varphi}^2\right),$$

while the kinetic energy of the $i-th$ lower pendulum can be expressed as:

$$\begin{aligned} T_{m_i} &= \frac{1}{2}m(\dot{x}_i^2 + \dot{y}_i^2 + \dot{z}_i^2) \\ &= \frac{1}{2}m\Big(L^2\cos^2\varphi\dot{\theta}^2 + H^2\cos^2\varphi_i\dot{\theta}_i^2 - 2HL\cos\varphi_i\sin[\theta-\theta_i]\sin\varphi\dot{\theta}_i\dot{\varphi} + L^2\dot{\varphi}^2 \\ &\quad +2HL\big(\cos\varphi\cos\varphi_i + \cos[\theta-\theta_i]\sin\varphi\sin\varphi_i\big)\dot{\varphi}\dot{\varphi}_i + H^2\dot{\varphi}_i^2 \\ &\quad +2HL\cos\varphi\dot{\theta}\big(\cos[\theta-\theta_i]\cos\varphi_i\dot{\theta}_i + \sin[\theta-\theta_i]\sin\varphi_i\dot{\varphi}_i\big)\Big), \end{aligned}$$

where $i = 1, 2$. Potential energy of the system is

$$V = g\big(L(2m+M)(1-\cos\theta\cos\varphi) + Hm(2-\cos\theta_1\cos\varphi_1 - \cos\theta_2\cos\varphi_2)\big).$$

The total energy of the system (Hamiltonian) $\mathcal{H}$ is equal to the sum of kinetic and potential energies of three considered pendula. Based on Lagrange equation of the second type one can derive six coupled second order ODEs. The equations of motion

of the upper pendulum are

$$L\cos\varphi\Big(gM\sin\theta - 2LM\sin\varphi\dot\theta\dot\varphi + LM\cos\varphi\ddot\theta + m\sum_{i=1}^{2}\Big(g\sin\theta + H\cos\varphi_i \times \sin[\theta-\theta_i]\dot\theta_i^2 - 2L\sin\varphi\dot\theta\dot\varphi - 2H\cos[\theta-\theta_i]\sin\varphi_i\dot\theta_i\dot\varphi_i + H\cos\varphi_i\sin[\theta-\theta_i]\dot\varphi_i^2 + L\cos\varphi\ddot\theta + H\cos[\theta-\theta_i]\cos\varphi_i\ddot\theta_i + H\sin[\theta-\theta_i]\sin\varphi_i\ddot\varphi_i\Big) = 0, \quad (1)$$

and

$$L\Big(gM\cos\theta\sin\varphi + LM\cos\varphi\sin\varphi\dot\theta^2 + LM\ddot\varphi + m\sum_{i=1}^{2}\Big(g\cos\theta\sin\varphi + L\cos\varphi\sin\varphi\dot\theta^2 + H\cos[\theta-\theta_i]\cos\varphi_i\sin\varphi\dot\varphi_i^2 - H\cos\varphi\sin\varphi_i\dot\varphi_i^2 + H\cos[\theta-\theta_i]\cos\varphi_i\sin\varphi\dot\theta_i^2 + H\ddot\varphi_i(\cos\varphi\cos\varphi_i + \cos[\theta-\theta_i]\sin\varphi\sin\varphi_i) + 2H\sin[\theta-\theta_i]\sin\varphi\sin\varphi_i\dot\theta_i\dot\varphi_i - H\sin[\theta-\theta_i]\cos\varphi_i\sin\varphi\ddot\theta_i + H\cos\theta\cos\varphi_i\sin\theta_i\sin\varphi\ddot\theta_i + L\ddot\varphi\Big) = 0. \quad (2)$$

The dynamics of the $i-th$ lower pendulum is also described by two second order ODEs:

$$Hm\cos\varphi_i\Big(g\sin\theta_i - 2H\sin\varphi_i\dot\theta_i\dot\varphi_i + H\cos\varphi_i\ddot\theta_i - L\Big(\cos\varphi\sin[\theta-\theta_i]\dot\theta^2 + 2\cos[\theta-\theta_i] \times \sin\varphi\dot\theta\dot\varphi + \cos\varphi\big(\sin[\theta-\theta_i]\dot\varphi^2 - \cos[\theta-\theta_i]\ddot\theta\big) + \sin[\theta-\theta_i]\sin\varphi\ddot\varphi\Big)\Big) = 0, \quad (3)$$

and

$$Hm\Big(g\cos\theta_i\sin\varphi_i + L\cos[\theta-\theta_i]\cos\varphi\sin\varphi_i\dot\theta^2 + H\cos\varphi_i\sin\varphi_i\dot\theta_i^2 - 2L\sin[\theta-\theta_i] \times \sin\varphi\sin\varphi_i\dot\theta\dot\varphi + L\big((-\cos\varphi_i\sin\varphi + \cos[\theta-\theta_i]\cos\varphi\sin\varphi_i)\dot\varphi^2 + \cos\varphi\sin[\theta-\theta_i] \times \sin\varphi_i\ddot\theta + (\cos\varphi\cos\varphi_i + \cos[\theta-\theta_i]\sin\varphi\sin\varphi_i)\ddot\varphi\big) + H\ddot\varphi_i\Big) = 0, \quad (4)$$

where $i = 1, 2$. These Eqs. (1)–(4) contains the full dynamics of the complete system, Fig. 1.

3 Nonlinear normal modes of the system

3.1 Eigenfrequencies

For a given level of energy (a set of initial conditions) three modes corresponding to the periodic solution of single spherical pendulum can be observed. Here, two rotational modes (symmetric) and one planar mode (where the pendulum swings in a vertical plane) are possible. In this paper we consider only rotational modes. For three coupled pendula and for low values of energy (in linear approximation) three rotational modes, each with own eigenfrequency, appear. To calculate these eigenfrequencies we apply the theory of linear normal modes. Let us assume that the amplitudes of motion of pendula are small, hence we can consider that the system performs harmonic oscillations. To linearize the systems we use the following approximations: $\sin\mathbf{q} = \mathbf{q}$

and $\cos \mathbf{q} = 1$, where $\mathbf{q} = [\varphi, \theta, \varphi_1, \theta_1, \varphi_2, \theta_2]^T$. For simplicity we can present the equations of motions, after linearization, in a matrix form:

$$\mathbf{A}\ddot{\mathbf{q}} + \mathbf{C}\mathbf{q} = 0, \tag{5}$$

where A and C are matrices of inertia and stiffness respectively, and they have got the following forms

$$\mathbf{A} = \begin{bmatrix} L^2(2m+M) & 0 & HLm & 0 & HLm & 0 \\ 0 & L^2(2m+M) & 0 & HLm & 0 & HLm \\ HLm & 0 & H^2m & 0 & 0 & 0 \\ 0 & HLm & 0 & H^2m & 0 & 0 \\ HLm & 0 & 0 & 0 & H^2m & 0 \\ 0 & HLm & 0 & 0 & 0 & H^2m \end{bmatrix}, \tag{6}$$

$$\mathbf{C} = \begin{bmatrix} gL(2m+M) & 0 & 0 & 0 & 0 & 0 \\ 0 & gL(2m+M) & 0 & 0 & 0 & 0 \\ 0 & 0 & gHm & 0 & 0 & 0 \\ 0 & 0 & 0 & gHm & 0 & 0 \\ 0 & 0 & 0 & 0 & gHm & 0 \\ 0 & 0 & 0 & 0 & 0 & gHm \end{bmatrix}. \tag{7}$$

For rotational modes, in three dimensional phase space, the periodic solutions are rotational ones around hanging down positions. For that reason we assume the solution of Eq. (5) as follows:

$$\mathbf{q} = \begin{bmatrix} \varphi \\ \theta \\ \varphi_1 \\ \theta_1 \\ \varphi_2 \\ \theta_2 \end{bmatrix} = \begin{bmatrix} \Psi_\varphi \sin[\omega t] \\ \Psi_\theta \cos[\omega t] \\ \Psi_{\varphi_1} \sin[\omega t] \\ \Psi_{\theta_1} \cos[\omega t] \\ \Psi_{\varphi_2} \sin[\omega t] \\ \Psi_{\theta_2} \cos[\omega t] \end{bmatrix} = \Psi \begin{bmatrix} \sin[\omega t] \\ \cos[\omega t] \\ \sin[\omega t] \\ \cos[\omega t] \\ \sin[\omega t] \\ \cos[\omega t] \end{bmatrix}, \quad \omega > 0, \quad t > 0, \forall \Psi_{j=\{1,2,3\}} \in \mathbb{R}. \tag{8}$$

For linear oscillations of the system we observe symmetry in two parallel planes (XY, YZ), hence $\Psi_\varphi = \Psi_\theta$, $\Psi_{\varphi_1} = \Psi_{\theta_1}$, $\Psi_{\varphi_2} = \Psi_{\theta_2}$. One can calculate the eigenfrequencies, ω, for which the periodic solutions are observed in the system, using the relation $(\mathbf{C} - \omega^2\mathbf{A})\Psi = 0$. Here the determinant $\det|C - \omega^2 A|$ has to vanish, which gives three independent frequencies

$$\begin{aligned} \omega_1 &= \sqrt{\frac{g}{H}}, \\ \omega_{2,3} &= \sqrt{\frac{g}{L}}\sqrt{a \pm b}, \end{aligned} \tag{9}$$

where $a = \frac{(H+L)(2m+M)}{2HM}$ and $b = \frac{\sqrt{2m+M}\sqrt{2(H+L)^2m+(H-L)^2M}}{2HM}$.

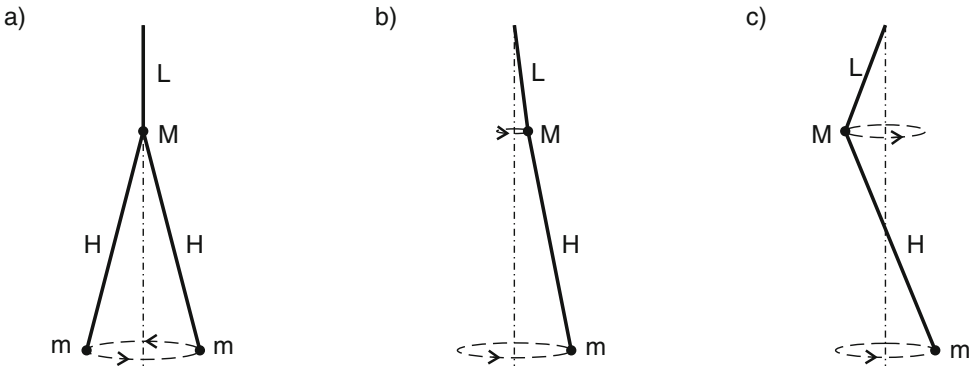

Fig. 2. The schematic representation of modes for (a) $\omega = \omega_1$ (b) $\omega = \omega_2$ and (c) $\omega = \omega_3$.

The schematic representation of motions corresponding to all three eigenfrequencies are shown in Fig. 2. Frequency ω_1 corresponds to the following solution: the phase shift between lower pendula is π, which causes a balance of forces acting on the upper pendulum, hence the upper pendulum is static (see Fig. 2a). For frequency ω_2 the upper and lower pendula rotate in-phase, lower pendula have the same amplitudes while the amplitude of upper pendulum is different (Fig. 2b). For frequency ω_3 the phase of upper pendulum is shifted by π compared to the phases of both lower pendula (Fig. 2c).

The eigenvectors, corresponding the eigenfrequencies condition $(C - \omega^2 A)\Psi = 0$, can be written as

$$\Psi_1 = \left[0, 0, \Psi_{\theta_1}, \Psi_{\theta_1}, -\Psi_{\theta_1}, -\Psi_{\theta_1}\right]^T,$$

$$\Psi_{2,3} = \left[\Psi_\theta, \Psi_\theta, \Psi_\theta(c \mp d), \Psi_\theta(c \mp d), \Psi_\theta(c \mp d), \Psi_\theta(c \mp d)\right], \tag{10}$$

where $c = \frac{(H-L)(2m+M)}{4Hm}$ and $d = \frac{\sqrt{2m+M}\sqrt{2(H+L)^2 m+(H-L)^2 M}}{4Hm}$.

3.2 Nonlinear normal modes

First we obtain eigenvectors using linear approximation theory. Each of them describes the periodic solution but only for the linearized system. When we have applied one of them to the nonlinear system, even assuming small energy ($\mathcal{H} \approx 0.02$) (Eqs. (1)–(4)) we obtain a quasiperiodic orbit (KAM tori) which is located close to the periodic solution of the linearized system. To correct the obtained solution, we have applied the Newton-Raphson algorithm. The integration of ODEs are performed with Runge-Kutta-Fehlberg (4,5) method. In numerical calculations we assume the following values of system parameters: $M = 2$, $m = 2$, $L = 1$, and $H = 3$. After substituting these values in Eqs. (9) we obtain the following linear eigenfrequencies: $\omega_1 = 1.732$, $\omega_2 = 1.553$ and $\omega_3 = 5.7959$. In Fig. 3a we present, on the frequency – energy plot, how the frequencies of three periodic solutions change with the increase of the total energy $\mathcal{H}$. Each branch is calculated in the following way: for starting point ($\mathcal{H} \approx 0.02$) we take initial conditions according to linear eigenvector, then we correct the obtained solution by Newton-Raphson scheme to periodic orbit. In next step this solution is perturbed (we add 1% of current total energy) so the energy is shifted to higher level and once again the correction is applied. The described procedure is repeated until the energy of the system reaches $\mathcal{H} = 300$.

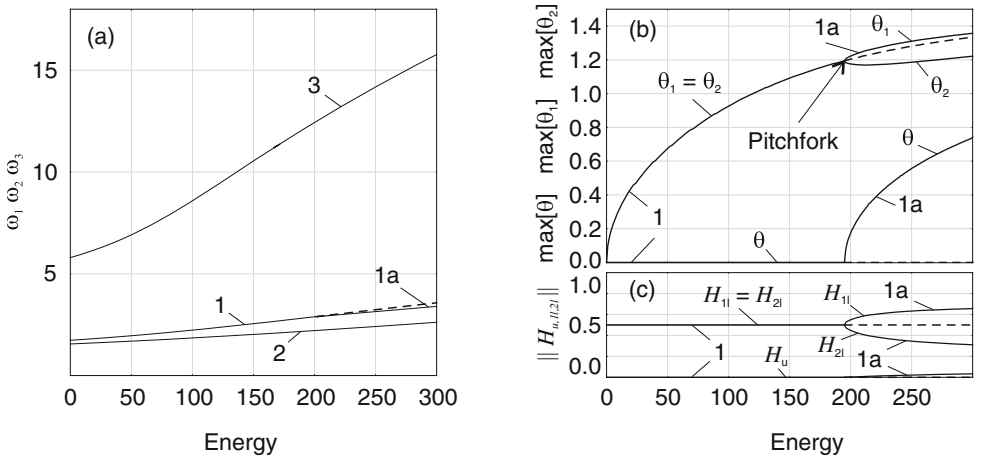

Fig. 3. (a) Frequency–energy plot of the investigated nonlinear system. Each branch begins with frequency calculated for linear system (No. 1 – ω_1, No. 2 – ω_2 and No. 3 – ω_3). (b) The maximum amplitudes of solutions as a function of energy for branches No. 1 and No. 1a. At $\mathcal{H} \sim 197$ we observe a pitchfork bifurcation which breaks the symmetry in the system, and hence the upper pendulum starts to oscillate ($\theta \neq 0$) and amplitudes of lower pendula (θ_1 and θ_2) have different values. (c) The normalized energies ($\|\mathcal{H}\| = 1$) for each pendulum as a function of total energy of the system for branches No. 1 and No. 1a. The solid and dashed lines correspond to respectively stable and unstable periodic solutions.

The successive increase of total energy $\mathcal{H}$ causes the increase of three frequencies, hence the periods of rotations become shorter. The maximum value of energy can be up to $\mathcal{H} = 300$ because the system has singular point at $\pi/2$. Therefore for branch No. 3 the maximum amplitude is close to $\pi/2$. Further increase of the energy ($\mathcal{H} > 300$) for branches No. 1, 1a and 2 causes only the increase of the amplitude and the rotational velocity, but no new phenomena are observed.

Branch No. 1 corresponds to clock-wise rotations of lower pendula with phase shifted by π while the upper one remains static (see Fig. 2a). However, with the increase of total energy we observe the change in the shape of periodic solutions (see Fig. 4) due to the presence of nonlinear terms in the equations of motion. For energy level equal to $\mathcal{H} = 197$ the symmetry breaking pitchfork bifurcation occurs. It is indicated by the appearance of No. 1a branch. After the bifurcation the frequencies of two solutions stay close in the whole range of considered energy. The changes of the maximum amplitudes of solutions along branches No. 1 and 1a are shown in Fig. 3b. The solid and dashed lines correspond respectively to stable and unstable periodic solutions. It is easy to see that, for branch No. 1a, the oscillations of lower pendula are asymmetric while the amplitude of the upper pendulum continuously increases. The amount of energy in each pendulum for branches No. 1 and No. 1a is presented in Fig. 3c. We normalize the total energy to one ($\|\mathcal{H}\| = 1$) and show its participation in each pendulum. It is easy to see that for branch No. 1 the energy is equally distributed between lower pendula. Since the upper pendulum is not moving before the bifurcation, and hence its energy is equal to zero. For branch No. 1a the energy of one lower pendulum starts to increase while the energy of the second one decreases. The energy of the upper pendulum also increaes after the bifurcation.

The change of the shape of periodic orbits for branches No. 1 (black line) and No. 1a (grey line) are shown in Fig. 4. In upper and lower rows, the trajectories of upper pendulum and lower pendula are presented respectively. For branch No. 1 the low energies solutions are nearly harmonic however for higher values of $\mathcal{H}$ we

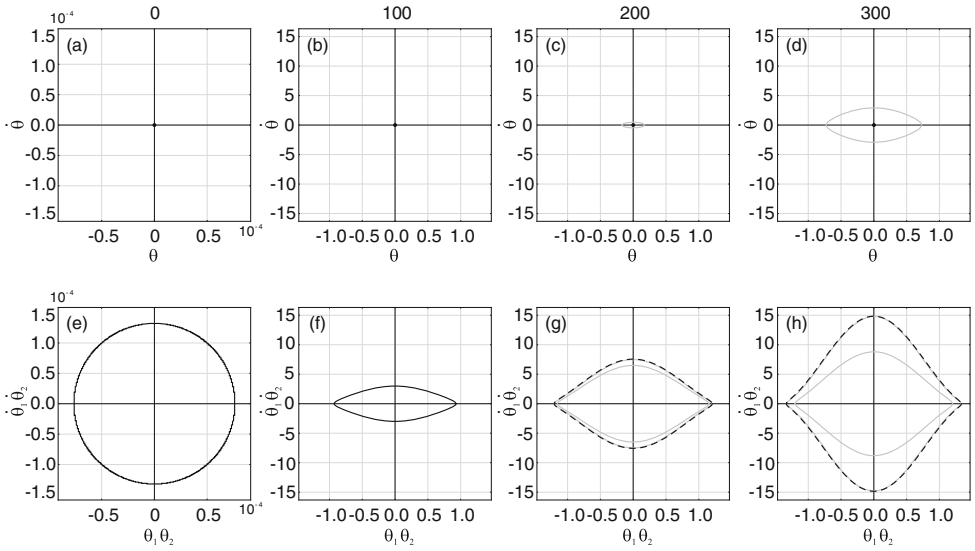

Fig. 4. The phase space trajectories of nonlinear normal modes along branches No. 1 and No. 1a. The total energy $\mathcal{H}$ is increased from left to right: $\mathcal{H} = 0.02$ (a, e), $\mathcal{H}$ =100 (b, f), $\mathcal{H} = 200$ (c, g) and $\mathcal{H} = 300$ (d, h). The upper and lower rows show the motions of upper and lower pendula respectively in phase space. The solid (stable solutions) and dashed (unstable solutions) black lines show periodic orbits along branch No. 1 while grey lines present the stable orbits along branch No. 1a.

observe the deformation around the maximum amplitude of pendula. Therefore, the time when the pendula are barely moving becomes longer in comparison to the rest period of oscillations. The periodic solution loses stability in pitchfork bifurcation (the continuous line changes to the dashed one) and the symmetry broken orbits appear (branch No. 1a).

For branch No. 2, corresponding to three pendula oscillating in-phase, we observe a slow increase of oscillation amplitude with the increase of total energy. The periodic solutions along branch No. 2 change their shapes similar to branch No. 1 (not presented here). For the third branch (No. 3) the upper pendulum rotates in anti-phase with lower pendula. The changes of periodic solutions shape are presented in Fig. 5. It is easy to see that, for low energy level, the orbits are nearly harmonic, while for higher levels of energy they become non-harmonic with visible nonlinear effects around the maximum amplitude. For $\mathcal{H} = 300$ the maximum amplitude of upper pendulum reaches the singular point $\theta = \pi/2$ (see 5a) therefore the motion for higher energy is impossible. In the case of branches No. 1 and No. 2 the amplitudes of lower pendula grow much faster than the amplitude of the upper one, while for branch No. 3 we observe an opposite behavior.

4 Energy transfer among pendula

In this section we present energy transfer between lower pendula via the upper pendulum. In the case of periodic solutions there is no energy transfer, i.e., the energy of each pendulum is constant. To observe the exchange of energy between the pendula one has to perturb the periodic motion. This is done by introducing a small mismatch in the initial conditions. For lower energy the periodic state leads to quasi-periodic motion (KAM tori) while for larger perturbations one can also observe chaotic

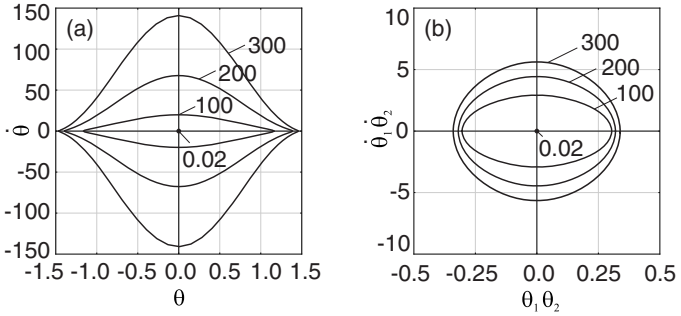

Fig. 5. The projections of trajectories in phase space of nonlinear normal modes of branch No. 3 for different energies: $\mathcal{H} = 0.02$, $\mathcal{H} = 100$, $\mathcal{H} = 200$ and $\mathcal{H} = 300$ of (a) upper and (b) lower pendula.

behavior. Additionally, in this section we take into account counter-rotating solutions as well. To achieve these we change the sign of the initial velocities ($\dot{\varphi}_2$ and $\dot{\theta}_2$) of one of lower pendula i.e. forcing one pendulum to move in the opposite direction. As discussed below, we observe that all counter-rotating solutions are chaotic.

4.1 Perturbation to first mode, ω_1

For low level of total energy ($\mathcal{H} = 0.017035$) we take the following initial conditions: $\theta = 0.0$, $\varphi = 0.0$, $\theta_1 = 0.012656702$, $\varphi_1 = 0.0$, $\theta_2 = -0.012656702$, $\varphi_2 = 0.0$, $\dot{\theta} = 0.0$, $\dot{\varphi} = 0.0$, $\dot{\theta}_1 = 0.0$, $\dot{\varphi}_1 = 0.02192759$, $\dot{\theta}_2 = 0.0$, $\dot{\varphi}_2 = -0.02192759$, which correspond to 1% perturbation of periodic solution. For counter-rotating the velocity of the second lower pendulum is equal to $\dot{\varphi}_2 = 0.02192759$ (the velocity $\dot{\theta}_2$ is equal to zero). In Fig. 6a,e,i we present how the energies of upper and lower pendula change in time for co-rotating (black line) and counter-rotating (grey line) without additional perturbation. For co-rotating motion the pendula do not transfer the energy between each other because of static upper pendulum, and synchronized periodic motions of lower pendula. For counter-rotating motion the lower pendula transfer energy via upper pendulum and motions are chaotic. For higher energy, after addition of small perturbation, i.e., $\delta\theta_1 = 0.01\theta_1$ and $\delta\dot{\varphi}_1 = 0.01\dot{\varphi}_1$ trajectories are shown in Fig. 6b,f,j. At this energy level the upper pendulum sets in motion independently from lower pendula. In both cases, either co- or counter, lower pendula exchange energy via the upper pendulum. The co-rotating solution does not remain periodic but it becomes quasiperiodic. For this level of perturbation the independent frequency is much smaller than the frequency of original periodic orbit, hence we observe a slow transfer of energy. However the counter-rotating motion remains chaotic. Note that the energy is transferred with the same frequency but the amplitude of upper pendulum's motion is much higher for counter-rotating than for co-rotating.

Shown in Fig. 6c,g,k are the trajectories for further high energy level, ($\mathcal{H} = 101.468$) with the following initial conditions: $\theta = 0.0$, $\varphi = 0.0$, $\theta_1 = 0.92996374$, $\varphi_1 = 0.0$, $\theta_2 = -0.92996374$, $\varphi_2 = 0.0$, $\dot{\theta} = 0.0$, $\dot{\varphi} = 0.0$, $\dot{\theta}_1 = 0.0$, $\dot{\varphi}_1 = 1.79562871$, $\dot{\theta}_2 = 0.0$, $\dot{\varphi}_2 = -1.79562871$. For counter-rotating case initial velocity of second pendulum is changed to $\dot{\varphi}_2 = 1.79562871$. The system behaves in similar way as in the low energy level cases. The only difference is in the amplitude of motion. However, for sufficiently high energy level, at ($\mathcal{H} =$????), as shown in Fig. 6d,h,l, we observe higher energy transfer between pendula for co-rotating case.

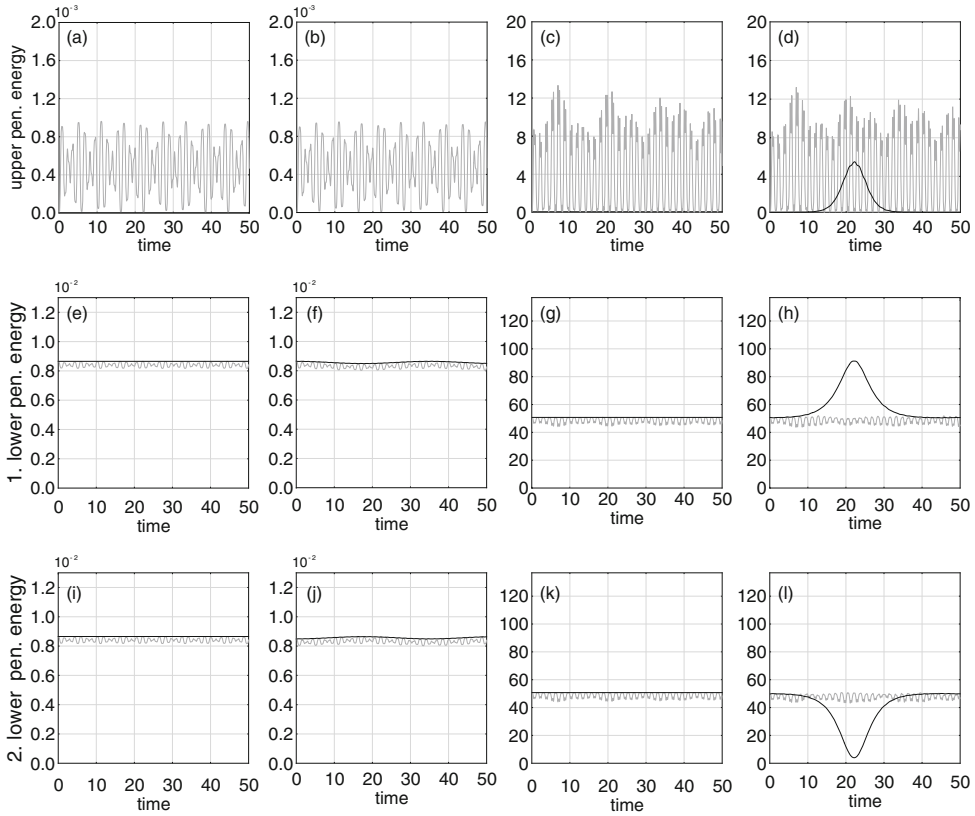

Fig. 6. The variation of energies as a function of time for the first mode, ω_1. The figures of upper row (a–d) correspond to the upper pendulum while the lower two rows (e–l) are for lower pendula. The black and grey lines in each figure represent co- and counter rotating solutions respectively. The trajectories for (a,e,i) low energy level with identical initial conditions, (b,f,j) low energy level with mismatched initial conditions, (c,g,k) high energy level ($\mathcal{H} = 100$) with identical initial conditions, and (d,h,l) high energy level ($\mathcal{H} = 100$) with mismatched initial conditions.

4.2 Perturbation to second mode, ω_2

For low energy level ($\mathcal{H} = 0.0778345$) the following initial conditions are taken: $\theta = 0.01745387$, $\varphi = 0.0$, $\theta_1 = 0.02384009$, $\varphi_1 = 0.0$, $\theta_2 = 0.02384009$, $\varphi_2 = 0.0$, $\dot{\theta} = 0.0$, $\dot{\varphi} = 0.02710668$, $\dot{\theta}_1 = 0.0$, $\dot{\varphi}_1 = 0.03702315$, $\dot{\theta}_2 = 0.0$, $\dot{\varphi}_2 = 0.03702315$. For counter-rotating the initial velocity of second pendulum $\dot{\varphi}_2 = -0.03702315$ (the velocity $\dot{\theta}_2$ is equal to zero) is considered. In Fig. 7a,e,i we show the change of energies as a function of time for periodic motion for co-rotating and chaotic oscillations for counter-rotating. For co-rotating case the pendula do not transfer the energy between each other. The upper pendulum is moving in-phase with lower pendula. When counter-rotating motion is observed lower pendula transfer energy to upper pendulum and vice verse. The fluctuation in energy indicates that motions are chaotic.

Next we add the following perturbation to initial conditions: $\delta\theta_1 = 0.01\theta_1$ and $\delta\dot{\varphi}_1 = 0.01\dot{\varphi}_1$. In Fig. 7b,f,j the change of energy in time for co-rotating and counter-rotating motions are presented. In both these cases lower pendula exchange energy via the upper one. Energy is transferred with the similar frequency but the amount of the exchanged energy is much bigger for counter-rotating case than for co-rotating.

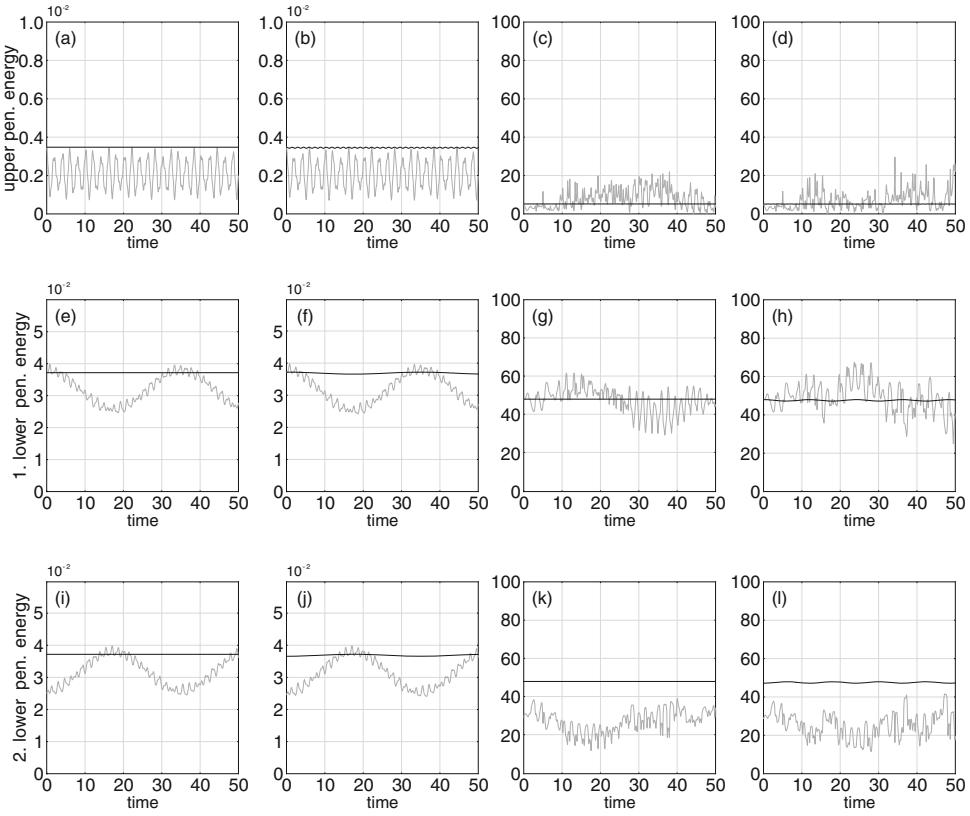

Fig. 7. The variation of energies as a function of time for the second mode, ω_2. The figures of upper row (a–d) correspond to the upper pendulum while the lower two rows (e–l) are for lower pendula. The black and grey lines in each figure represent co- and counter rotating solutions respectively. The trajectories for (a,e,i) low energy level with identical initial conditions, (b,f,j) low energy level with mismatched initial conditions, (c,g,k) high energy level ($\mathcal{H} = 100.989$) with identical initial conditions, and (d,h,l) high energy level ($\mathcal{H} = 100.989$) with mismatched initial conditions.

For higher energy level ($\mathcal{H} = 100.989$) the following initial conditions are considered: $\theta = 0.66836221$, $\varphi = 0.0$, $\theta_1 = 0.817659$, $\varphi_1 = 0.0$, $\theta_2 = 0.817659$, $\varphi_2 = 0.0$, $\dot{\theta} = 0.0$, $\dot{\varphi} = 1.14578007$, $\dot{\theta}_1 = 0.0$, $\dot{\varphi}_1 = 1.3488661$, $\dot{\theta}_2 = 0.0$, $\dot{\varphi}_2 = 1.3488661$. The trajectories are shown (Fig. 7c,g,k). For counter-rotating case the initial velocity of the second pendulum is changed to $\dot{\varphi}_2 = -1.3488661$. For higher energy counter-rotating continues to shows chaotic motion (Fig. 7d,h,l). In the co-rotating case lower pendula oscillate in quasiperiodic way. However, for higher energy level (($\mathcal{H} = 100.989$)), the period of energy transfer is much shorter than for lower total energy level.

4.3 Perturbation to third mode, ω_3

Now we consider the third mode where upper and lower pendula move in opposite directions. For low energy level ($\mathcal{H} = 0.0208567$) with the following initial conditions $\theta = 0.017453269$, $\varphi = 0.0$, $\theta_1 = -0.0063880017$, $\varphi_1 = 0.0$, $\theta_2 = -0.0063880017$,

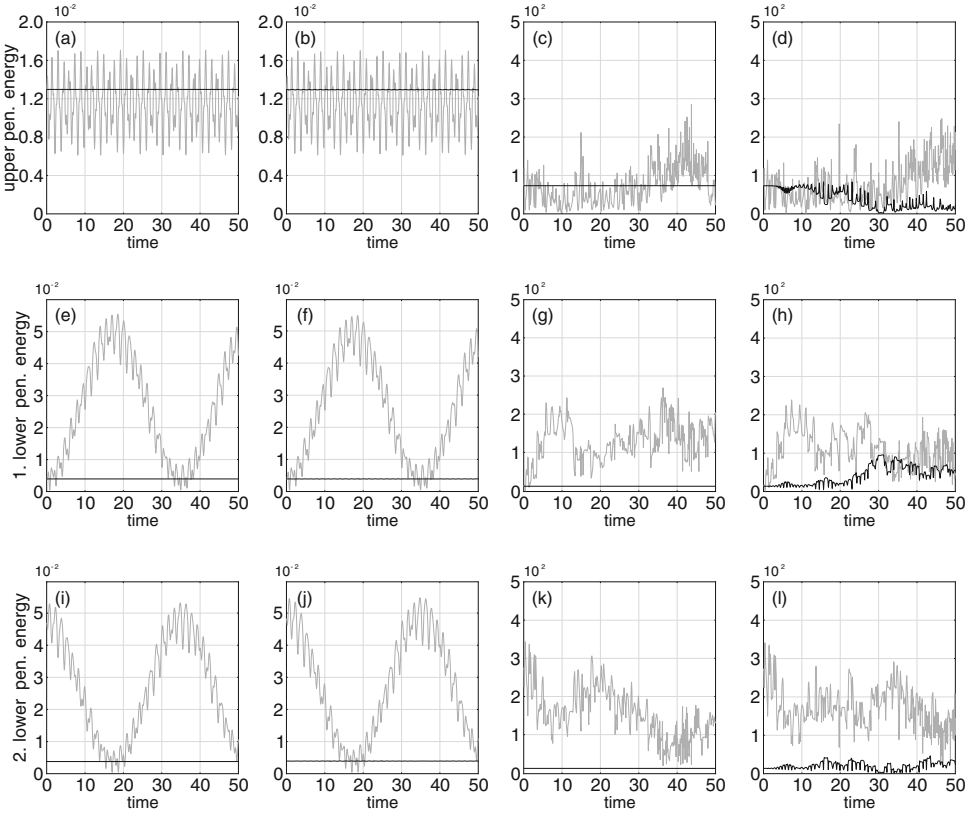

Fig. 8. The variation of energies as a function of time for the third mode, ω_3. The figures of upper row (a–d) correspond to the upper pendulum while the lower two rows (e–l) are for lower pendula. The black and grey lines in each figure represent co- and counter rotating solutions respectively. The trajectories for (a,e,i) low energy level with identical initial conditions, (b,f,j) low energy level with mismatched initial conditions, (c,g,k) high energy level ($\mathcal{H} = 100.898$) with identical initial conditions, and (d,h,l) high energy level ($\mathcal{H} = 100.898$) with mismatched initial conditions.

$\varphi_2 = 0.0$, $\dot{\theta} = 0.0$, $\dot{\varphi} = 0.10115284$, $\dot{\theta}_1 = 0.0$, $\dot{\varphi}_1 = -0.037024141$, $\dot{\theta}_2 = 0.0$, $\dot{\varphi}_2 = -0.037024141$ are taken. For counter-rotating we assume $\dot{\varphi}_2 = 0.037024141$ (Fig. 8a,e,i) Co-rotating solution is periodic and pendula do not exchange energy between each other. In counter-rotating case we can observe chaotic beating. Similar behavior is observed for higher energy level ($\mathcal{H} = 100.898$) as shown in Fig. 8b,f,g. and $\delta\dot{\varphi}_1 = 0.01\dot{\varphi}_1$. The energy transfer is more for counter-rotating than for co-rotating.

At high energy level ($\mathcal{H} = 100.898$) with initial conditions: $\theta = 1.16073984$, $\varphi = 0.0$, $\theta_1 = -0.32498693$, $\varphi_1 = 0.0$, $\theta_2 = -0.32498693$, $\varphi_2 = 0.0$, $\dot{\theta} = 0.0$, $\dot{\varphi} = 7.90726534$, $\dot{\theta}_1 = 0.0$, $\dot{\varphi}_1 = -2.75298937$, $\dot{\theta}_2 = 0.0$, $\dot{\varphi}_2 = -2.75298937$ (Fig. 8c,g,k). For counter-rotating case, the initial velocity of second pendulum is changed to $\dot{\varphi}_2 = 2.75298937$. In these both cases, co- and counter-rotating oscillations of pendula are chaotic for higher total energy level (Fig. 8d,h,l).

5 Summary

In this paper we study the dynamics of three coupled conservative spherical pendula. The analytical calculations of the eigenfrequencies of the linearized system, allow us to identify three independent linear modes of the pendulum's rotation. For all of them, pendula rotate in clock-wise direction with different phase shifts. The obtained linear modes allow us to compute the nonlinear normal modes for increasing energy in the system using the path-following method. As it is expected with growing total energy the frequencies of modes increase. In the first mode we observe a pitchfork bifurcation, which causes the appearance of symmetry broken periodic solution and destabilization of the initial one.

In the case of periodic motion there is no energy transfer between the pendula, but even a small perturbation of periodic initial conditions leads to the exchange of energy. We show the energy flows for each mode considering two cases of rotations – in clock-wise and counter clock-wise directions. In the first case for all three modes we observe the dynamics on a KAM tori. The period of energy transfer is much longer than the natural period of each mode. In the second case the dynamics is always chaotic.

This work has been supported by the Foundation for Polish Science, Team Programme under project TEAM/2010/5/5 (BW, PP, TK). AP would like to thank the DST, Govt. of India for financial support.

References

1. A. Pikovsky, M. Rosenblum, J. Kurths (Cambridge University Press, 2001)
2. S.H. Strogatz, Physica D: Nonlinear Phenom. **143**, 1 (2000)
3. Y. Kuramoto (Springer, 1984)
4. S. Sabarathinam, K. Thamilmaran, L. Borkowski, P. Perlikowski, P. Brzeski, A. Stefanski, T. Kapitaniak, Commun. Nonlinear Sci. Num. Simul. **18**, 3098 (2013)
5. S. Yanchuk, K. Schneider, *Proceedings of Equadiff 2003* (World Sci., 2005), p. 494
6. A. Vakakis, O. Gendelman, L. Bergman, D. McFarland, G. Kerschen, Y. Lee, Vol. 156 (Springer, 2008)
7. G. Saxena, A. Prasad, R. Ramaswamy, Phys. Reports **521**, 205 (2012)
8. N.E. Wierschem, D.D. Quinn, S.A. Hubbard, M.A. Al-Shudeifat, D.M. McFarland, J. Luo, L.A. Fahnestock, B.F.S. Jr., A.F. Vakakis, L.A. Bergman, J. Sound Vib. **331**, 5393 (2012)
9. G. Rega, S. Lenci, B. Horton, M. Wiercigroch, E. Pavlovskaia, Int. J. Bif. Chaos **22**, 1250100 (2012)
10. K. Czolczynski, P. Perlikowski, A. Stefanski, T. Kapitaniak, Chaos: An Interdisciplin. J. Nonlinear Sci. **21** (2011)
11. P. Brzeski, P. Perlikowski, S. Yanchuk, T. Kapitaniak, J. Sound Vib. **331**, 5347 (2012)
12. M.G. Olsson, Am. J. Phys. **46**, 1118 (1978)
13. M.G. Olsson, Am. J. Phys. **49**, 531 (1981)
14. R. Cushman, J.J. Duistermaat, Bull. (New Ser.) Am. Math. Soc. **19**, 475 (1988)
15. V. Guillemin, A. Uribe, Commun. Math. Phys. **122**, 563 (1989)
16. S. Leyendecker, P. Betsch, P. Steinmann, Comput. Mech. **33**, 174 (2004)
17. P.H. Richter, H.R. Dullin, H. Waalkens, J. Wiersig, J. Phys. Chem. **100**, 19124 (1996)
18. T. Lee, M. Leok, N. Harris McClamroch, ArXiv e-prints [`arXiv:1103.2822`] (2011)
19. C.M. Bender, B.K. Berntson, D. Parker, E. Samuel, Am. J. Phys. **81**, 173 (2013)
20. H.C. Mayer, R. Krechetnikov, Phys. Rev. E **85**, 046117 (2012)
21. A. Steindl, H. Troger, *Bifurcation: Analysis, Algorithms, Applications* (Birkhauser Basel, 1987), p. 277

22. J.E. Marsden, J. Scheurle, Z. Ang. Math. Phys. ZAMP **44**, 17 (1993)
23. P. Chossat, N. Bou-Rabee, SIAM J. Appl. Dyn. Syst. **4**, 1140 (2005)
24. S. Hu, E. Leandro, M. Santoprete, Reg. Chaotic Dyn. **17**, 36 (2012)
25. S. Shaw, C. Pierre, J. Sound Vib. **164**, 85 (1993)
26. G. Kerschen, M. Peeters, J.-C. Golinval, A.F. Vakakis, Mech. Syst. Signal Process. **23**, 170 (2009)
27. M. Peeters, R. Viguié, G. Sérandour, G. Kerschen, J.-C. Golinval, Mech. Syst. Signal Process. **23**, 195 (2009)